Electrostatics and the Gating Pore of *Shaker* Potassium Channels

Leon D. Islas and Fred J. Sigworth

From the Department of Cellular and Molecular Physiology, Yale University School of Medicine, New Haven, Connecticut 06520

ABSTRACT Various experiments have suggested that the S4 segment in voltage-dependent Na^+ and K^+ channels is in contact with a solvent-accessible cavity. We explore the consequences of the existence of such a cavity through the electrostatic effects on the gating currents of *Shaker* K^+ channels under conditions of reduced ionic strength *S*. We observe that ~10-fold reductions of intracellular *S* produce reductions of the measured gating charge of ~10%. These effects continue at even lower values of *S*. The reduction of gating charge when *S* is reduced by 10-fold at the extracellular surface is much smaller (~2%). Shifts of the $Q(V)$ curve because of a reduced *S* are small (<10 mV in size), which is consistent with very little fixed surface charge. Continuum electrostatic calculations show that the *S* effects on gating charge can be explained by the alteration of the local potential in an intracellular conical cavity of 20–24-Å depth and 12-Å aperture, and a smaller extracellular cavity of 3-Å depth and the same aperture. In this case, the attenuation of the membrane potential at low *S* leads to reduction of the apparent gating charge. We suggest that this cavity is made by a bundle of transmembrane helices, and that the gating charge movement occurs by translocation of charged residues across a thin septum of ~3–7 Å thickness.

KEY WORDS: Gating currents • voltage dependence • Poisson-Boltzmann equation

INTRODUCTION

Gating of voltage-dependent channels occurs by the interaction of the membrane electric field with charged residues in the channel protein. It now seems clear that the main voltage-sensing elements are the charges of basic amino acid residues in the S4 transmembrane domain, and that gating involves movement of the S4 in the membrane potential field. This movement has been measured indirectly by monitoring state-dependent modification of introduced cysteines or directly by voltage clamp fluorometry (Yang and Horn, 1995; Mannuzzu et al., 1996; Yang et al., 1996; Cha and Bezanilla, 1997). The charge movement produced by this conformational change in Na^+ and K^+ channels has been measured to be in the range of 7–13 e_o (Hirschberg et al., 1995; Aggarwal and MacKinnon, 1996; Seoh et al., 1996; Islas and Sigworth, 1999).

Early theories of how the S4 is able to transduce a voltage change into a conformational change assumed an α-helical conformation and had the segment undergoing a screw-like outward motion. This interpretation makes use of the assumption that the large charge movement has to be produced by the interaction of the voltage sensor with an electric potential that is imposed across the full thickness of the plasma membrane, roughly 30 Å. For example, four 25-Å-long α-helices with four equally spaced positive charges in a linear field on a 25-Å membrane would have to be displaced almost 20 Å normal to the membrane plane to produce 12 e_o of gating charge. Such a translocation of an α helix is a conformational change of unprecedented magnitude in a membrane protein.

It has been demonstrated that the accessibility of introduced cysteine residues in S4 to soluble sulfhydryl modifying agents is state-dependent and occurs in a manner consistent with the movement of the S4 voltage sensor, transporting residues from the intracellular to the extracellular face of the channel upon depolarization (Yang and Horn, 1995; Larsson et al., 1996; Baker et al., 1998). In view of the accessibility patterns of the S4 in the Na^+ channel, Yang and Horn (1995) proposed that the S4 is actually located in a water-filled cavity contiguous with the intracellular solution that has been called the gating pore or "canaliculus" (Goldstein, 1996). Larsson et al. (1996) demonstrated that in the *Shaker* S4, modification of introduced cysteines is consistent with a picture in which the S4 is able to move a small distance and still produce the large charge movement measured. These observations implied that the membrane potential might be highly focused in a small region around the S4 and that as in the Na^+ channel, a region of high dielectric constant might surround the *Shaker* S4. In a remarkable set of experiments, Starace et al. (1997) provided evidence that the region in which most of the membrane potential falls across the channel must be very small to account for experiments in which a single histidine substitution al-

Address correspondence to Fred J. Sigworth, Department of Cellular and Molecular Physiology, Yale University School of Medicine, 333 Cedar Street, New Haven, CT 06520; Fax: (203) 785 4951; E-mail: fred.sigworth@yale.edu

TABLE I

Composition of Solutions

Solution	Pipet normal	Pipet K	Intracellular K	Intracellular control		Intracellular			Extracellular control	Extracellular	
				NMDG	Cs	24	12	12 (Cs)		28	16
K-Asp	0	150	150	0	0	0	0	0	0	0	0
NMDG-Asp	140	0	0	148	0	0	2	0	150	0	0
KCl	5	2	2	2	0	5	0	0	5	10	2
CsCl	0	0	0	0	150	0	0	2	0	0	0
HEPES	5	5	5	5	5	5	5	5	10	10	5
EGTA	0	0	5	5	5	5	2	2	0	0	0
$MgCl_2$	2	2	1	1	1	1	1	1	2	1	1
$CaCl_2$	1.8	1.8	0	0	0	0	0	0	1	1	1
Sucrose	0	0	0	0	0	295	300	300	0	295	300
*S**	305	319	318	318	318	24	12	12	325	28	16

Composition of solutions used in these experiments; concentrations are given in mM. The pH was adjusted to 7.3 for intracellular solutions and 7.4 for extracellular solutions. At these pH values, Ca-EGTA is mainly divalent and HEPES is a zwitterion (neutral). The measured osmolarity of the solutions ranged from 340 to 355 mOsm/kg. *Values are measured in millimolar.

lows for proton transport in a pH gradient, as if the histidine completed a narrow pore. Taken together, all of this evidence seems to suggest that the membrane potential is highly focused in a small region around the S4, and that the space around the S4 may be surrounded by a solute-accessible region. These may be clever design elements necessary to obtain a large charge movement with a relatively small conformational change, since the gating charges would then traverse only a small distance to be translocated across most of the membrane potential.

If this arrangement of a water-filled region around the voltage sensor is correct, the electric field may have a complicated shape in the gating pore. For example, it has been demonstrated that cavities within water-soluble proteins produce large focusing effects of the local electric field and that the effects of ionic strength and pH on the electric field in these cavities can be large (Klapper et al., 1986; Rashin et al., 1986). In an integral membrane protein such as an ion channel, the ionic strength of the electrolyte solution in the extracellular and intracellular regions determines the Debye length and, thus, affects the local electric field. If some of the voltage sensing charges lie in cavities, it is possible that altering the local electrical field by manipulation of ionic strength could affect the size of the effective gating charge.

In the experiments presented in this report, we seek to investigate the effects of low ionic strength on charge movement of the *Shaker* potassium channel, and possibly to estimate the size of the cavity in which the voltage sensor lies. We investigate, through calculations with the linearized Poisson-Boltzmann equation, the size of the ionic screening effects on a simulated gating pore and seek to interpret these in terms of possible geometries for the proposed gating pore.

MATERIALS AND METHODS

Channels and Oocyte Preparation

The inactivation-removed *Shaker* 29-4 channel ShΔ (Hoshi et al. 1990) and the nonconducting W434F mutant ShΔF, (Perozo et al., 1993) were subcloned in the vector pGEM and linearized with NotI. In vitro transcription was done with T7 polymerase, and mRNA was stored at a concentration of 1 μg/μl.

Xenopus laevis oocytes were harvested under anesthesia and defolliculated by incubation with collagenase 1A in Ca^{2+}-free OR2 media for 1 h. Oocytes were kept at 20°C in a solution ([in mM]: 96 NaCl, 1.8 $CaCl_2$, 1 $MgCl_2$, and 5 HEPES), and injected 1 or 2 d after harvesting with 50 nl of mRNA with a Nanostepper (Drummond Co.) using pipets of 20-μm diam. Oocytes were used in experiments 1–7 d after injection.

Solutions

Low *S* solutions were prepared with sucrose or mannitol to maintain osmolarity and avoid osmotic water transport across the membrane that could produce concentration gradients. The concentration of divalent ions was kept constant in both high and low *S* solutions to avoid specific effects. We tried as much as possible to keep the same concentration of permeant ions to circumvent their known effects on gating. The composition of solutions is listed in Table I.

Electrical Recordings

Gating currents from ShΔF and ionic currents from ShΔ channels were recorded in the inside-out patch configuration for testing the effects of ionic strength on the intracellular side of the channel, whereas the cut-open oocyte technique and conventional two-electrode voltage clamp were used to examine extracellular effects. Patches were obtained from mRNA-injected oocytes using borosilicate glass pipets that had a resistance of 1–4 MΩ. Patches were excised into a control solution and locally perfused using a pipet of 20–50 μm in diameter positioned ~10 μm from the patch. Currents were filtered at 5 kHz (−3 dB Bessel characteristic) and sampled at 100 kHz using an EPC-9 amplifier

(HEKA Elektronik). 20 or more sweeps were averaged. Linear leak and capacitive currents were subtracted using a −P/4 protocol with a leak holding potential of −120 mV.

Cut-open oocyte voltage clamp recording was done with an amplifier (model CA-1B; Dagan Corp.). A modification to the external solution perfusion system in the cut-open chamber was used. The top and guard chambers were perfused at the same time to avoid gradients in solution composition between these chambers. For two-microelectrode voltage clamp, a Warner Instruments amplifier (OC-725) was used. Current and voltage microelectrodes had a resistance of 400 kΩ, and were filled with 1 M KCl.

Data Analysis

Estimation of the number of channels in a patch of membrane was done by nonstationary noise analysis (Sigworth, 1980; Heinemann and Conti, 1992). The mean and variance were calculated from 50 to 60 current traces elicited by depolarizing steps to the indicated membrane potential filtered at 5 kHz. Pulses were delivered at 0.5-s intervals. The variance estimation made use of groups of four sweeps to reduce the influence of drifting baselines and channel rundown. The pulsed data were displayed in the form of mean–variance relationships and fitted to the equation

$$\sigma^2 = iI - \frac{I^2}{N},$$

where σ^2 is the variance, I is the mean current, i is the single channel current, and N is the number of channels. The maximal open probability was then obtained as

$$p_{max} = \frac{I_{max}}{Ni}.$$

For estimation of the gating current noise, the nonstationary variance was calculated from 1,000 sweeps (in groups of four) to minimize the effects of the baseline current drift. Data were sampled at 100 kHz and filtered at 5 kHz. $Q(V)$ data were fitted to a Boltzmann function of the form:

$$Q(V) = \frac{Q_{max}}{1 + \exp[-q_g(V - V_{0.5})/kT]},$$

where Q_{max} is the charge at saturated voltages, $V_{0.5}$ is the voltage of half activation and q_g is the effective charge; kT has its usual meaning. Values are expressed as the mean ± standard error.

Simulations

The linearized Poisson-Boltzmann equation (see Eq. 5) was solved analytically for the one-dimensional case. For the more complex geometries, it was solved numerically in cylindrical coordinates using the finite difference algorithm of Jordan et al. (1989). The implementation was done using Matlab (The Math Works, Inc., version 5) running on a Macintosh G3 computer. Proper convergence, using a grid size of 0.5 Å in both the radial (r) and the z direction, was reached in 16,000 iterations, and took ~4 min for a grid of 60 × 110 Å. The boundary conditions were set such that the potential at the bottom of the integration box, which corresponds to the intracellular solution, is unity and at the top (extracellular solution) it is zero. The radial component of the electric field was also set to zero at the cylindrical (r = 60 Å) boundary. The integration was carried out to 40 Å beyond the membrane in the intracellular and extracellular solutions. The accuracy of the calculation was checked by solving for a point charge and comparing with the analytical expression for the point-charge problem (Bockris and Reddy, 1973).

RESULTS

Electrostatic Effects of Ionic Strength on Shaker Gating Currents

The experimentally measured charge movement from gating currents is the product of the moving charge and its coupling to the local electrostatic potential (Sigworth, 1994). The charge in an arbitrary state λ of the channel is given by

$$Q_\lambda = \sum_i q_i \delta_{i\lambda}, \quad (1)$$

where the sum is over all the charges q_i of the protein in state λ. The quantity $\delta_{i\lambda}$ is given by

$$\delta_{i\lambda} = \left.\frac{\partial \phi_i(\lambda, V)}{\partial V}\right|_{V=0}. \quad (2)$$

Thus, $\delta_{i\lambda}$ is the "electrical distance" of the i^{th} charge, and represents the degree of coupling between the local potential ϕ_i and the membrane potential V. The steady-state charge measured in the external circuit at a membrane potential V depends on the state occupancies p_λ according to

$$Q_{ext} = \sum_{\lambda=1}^{n} p_\lambda V \cdot Q_\lambda. \quad (3)$$

The measured charge movement is then given by

$$Q(V) = Q_{ext}(V) - Q_{ext}(V_o), \quad (4)$$

where V_o is a reference potential typically chosen to have the channels in a fully deactivated state. It can be seen that only charges q_i that move relative to the electric field ($\delta_{i\lambda}$ changes with changes in λ) contribute to $Q(V)$. Any manipulation that alters the relationship between V and ϕ_i (and therefore changes $\delta_{i\lambda}$) can change the magnitude of Q. The magnitude of the change in the local potential is expected to be a function of the physical conformation of the channel and the lipid bilayer.

We set out to investigate the effects of the electrostatic environment on the gating charge movement in *Shaker* K^+ channels through manipulation of the ionic strength (S), and interpret the results in terms of the possible local environment and conformation of the S4 voltage sensor.

The Electrical Potential Distribution in Lipid Bilayer Membranes

If a potential difference is imposed across a lipid bilayer, bathed in both sides by an electrolyte solution,

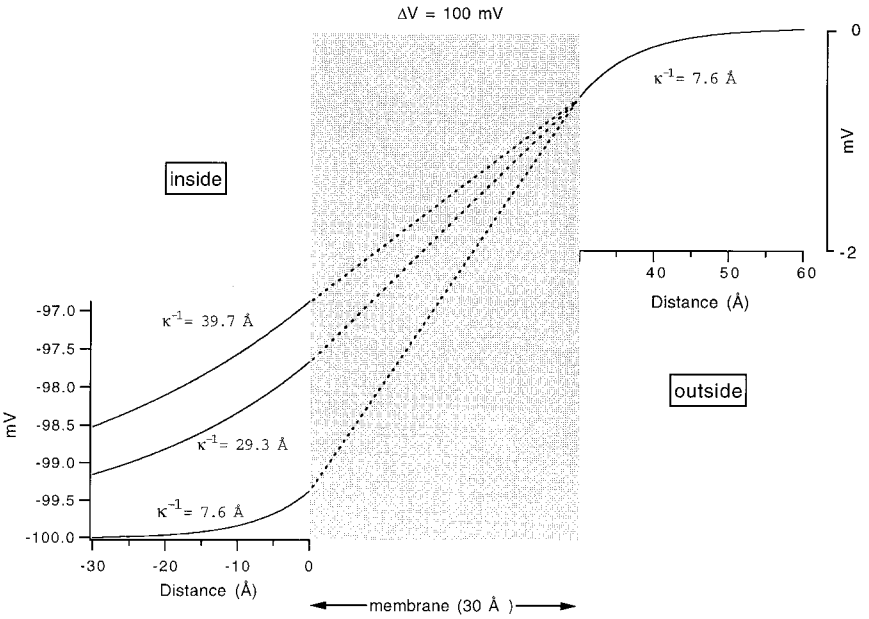

FIGURE 1. Analytical solution of the linearized Poisson-Boltzmann equation for a planar membrane of 30 Å thickness. The ionic strength in the outside solution is fixed at 318 mM (κ^{-1} = 7.6 Å) and, in the intracellular side, it is reduced from 318 to 24 mM (κ^{-1} = 29.1 Å) and 12 mM (κ^{-1} = 39.7 Å). The imposed membrane potential is −100 mV. The fraction of membrane potential that decays in the intracellular bath is 0.75, 2.1, and 2.8% of the total potential, respectively. The potential decays exponentially on the internal and external side of the membrane and linearly in the membrane region. Note the different scales used to represent the potential in the solutions and in the membrane.

the potential adopts a characteristic distribution. The potential inside the lipid bilayer decays as a linear function of distance. Outside the membrane, in the electrolyte solution, it decays as an exponential function of distance, because of the redistribution of mobile ions in solution. This is best illustrated by a continuum calculation based on classical electrostatics. The electrical potential in a region of space can be described by the macroscopic Poisson-Boltzmann equation. For small potentials, the linearized Poisson-Boltzmann equation holds, which in the case of zero fixed surface charge density has the form

$$\nabla \cdot [\varepsilon \nabla \phi] - \varepsilon \phi \kappa^2 = 0, \tag{5}$$

where ϕ represents the space-dependent electrical potential, ε is the space-dependent dielectric constant, and the decay constant κ^2 is given by

$$\kappa^2 = \frac{4\pi e_o^2}{\varepsilon kT} \sum_i c_i z_i^2, \tag{6}$$

where κ^{-1} has units of distance and is called the Debye length; c_i is the concentration of ionic species i, and z_i is the valence.

Roux (1997) has obtained an analytical solution to the linearized Poisson-Boltzmann equation in one dimension for a membrane potential V, in a membrane of thickness d by matching the boundary conditions to make ϕ and $\varepsilon \nabla \phi$ continuous across the membrane boundaries. Let $z = 0$ be the inner membrane boundary and $z = d$ be the outer membrane boundary, then the analytical expressions for ϕ are:

$$\phi = \begin{cases} \dfrac{V}{\dfrac{\varepsilon_s}{\varepsilon_m}\kappa d + 2} e^{(\kappa z)}, & z < 0 \\ V\left(\dfrac{\dfrac{\varepsilon_s}{\varepsilon_m}\kappa z + 1}{\dfrac{\varepsilon_s}{\varepsilon_m}\kappa d + 2}\right), & 0 \le z \le d \\ V - \dfrac{V}{\dfrac{\varepsilon_s}{\varepsilon_m}\kappa d + 2} e^{-\kappa(z-d)}, & z > d \end{cases} \tag{7}$$

ε_s and ε_m are the dielectric constants of the solution and the membrane, respectively. Using this analytical expression, the potential distribution across a lipid bilayer of thickness d = 30 Å was calculated, when a potential of −100 mV is imposed across it (Fig. 1). The potential in the membrane decays linearly, and the potential in the bath decays according to the Debye-Hückel exponential. The fraction of the transmembrane potential that decays in the bath is a function of the electrostatic shielding of the solution. For a 1:1 electrolyte and ε_s = 80, the Debye length is given by

$$\kappa^{-1} = \frac{137\,\text{Å} \cdot \text{mM}^{1/2}}{\sqrt{S}},$$

where S is the ionic strength, which is given by

$$S = \sum_i c_i \cdot z_i^2,$$

where c_i and z_i are the concentration and the valence of ion i, respectively.

In the case of a physiological solution with S = 300 mM, only 0.75% of the total potential decays in the so-

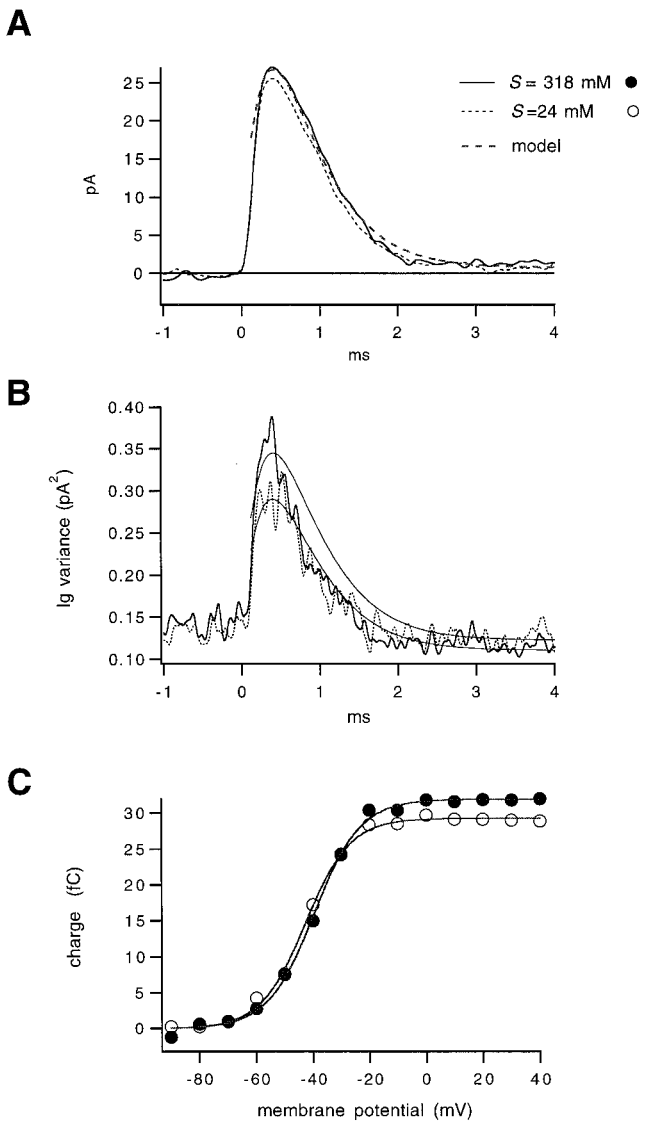

FIGURE 2. Effects of low ionic strength solution (24 mM) on the gating charge movement in *Shaker*. (A) Gating current traces at +20 mV from a holding potential of –90 mV, before (continuous trace) and after (dotted trace) perfusion on the intracellular side of a patch. The dashed curve is the gating current predicted by the model, corresponding to the high *S* current. (B) The variance of the gating current at +20 mV calculated from fluctuation analysis of the gating current. The continuous trace is the variance in the control solution, and the dotted trace is the variance in the low ionic strength solution. A reduction of 10% in the charge predicts a reduction of 20% in the gating charge variance. The light curves superimposed in the variance are the prediction according to Eq. 8. The gating current was calculated according to the simple irreversible scheme:

$$C_o \xrightarrow{\alpha, q_1} C_1 \xrightarrow{\beta, q_2} O$$

SCHEME 1.

with $\alpha = 2{,}380\ s^{-1}$, $q_1/q_2 = 0.011 e_o$, and $\beta = 2440\ s^{-1}$ for the high ionic strength; and $\alpha = 2{,}500\ s^{-1}$, $q_1/q_2 = 0.005$, and $\beta = 2390\ s^{-1}$ for low ionic strength. (C) The $Q(V)$ relationship for the patch in A. Open symbols are the charge in low ionic strength (24 mM) and closed symbols are the control (318 mM). Continuous curves are fits to the Boltzmann activation function (see MATERIALS AND METHODS). The following are parameters of the fit for 24 mM: $Q_{max} = 29.3$ fC, $V_{0.5} = -42.6$ mV, and $q_g = 3.1\ e_o$. For 318 mM: $Q_{max} = 31.9$ fC, $V_{0.5} = -39.6$ mV, and $q_g = 3.0\ e_o$.

lution. When *S* is reduced to 20 or 10 mM, the fraction of potential decaying in the solution increases to 2 and 2.8%, respectively (Fig. 1). Thus, if the charge movement occurs by displacement of the gating charge from one side to the other of the membrane, then in the case of low *S*, less potential will drop across the membrane itself. This will produce a reduction in the $\delta_{i\lambda}$ and, in consequence, a slight reduction in the measured charge movement. A more complicated situation is to be expected if the charge movement does not involve simple displacement of charged residues from one side of the membrane to the other. As was discussed previously, a clear view of the 3-D organization of transmembrane segments is lacking, but cysteine modification experiments suggest that most of the S4 residues are accessible to the aqueous phase. These results lead to the idea that the S4 transmembrane segment may be surrounded by a solvent-accessible cavity. If this is the case, one expects a larger reduction of the charge with low values of *S*, and the magnitude of the reduction will be a function of the shape of the cavity.

Intracellular Ionic Strength Effects

The mutant *Shaker* channel ShΔF was used to record gating currents. This construct contains the W434F mutation that suppresses ionic currents by promoting an inactivation process while leaving the voltage-dependent activation process relatively untouched, allowing for recordings of charge movement without the use of a blocking agent (Perozo et al., 1993; Yang et al., 1997). Currents were recorded in the inside-out configuration of the patch-clamp technique, and the intracellular face was exposed to low *S* solutions. The tonicity of the solutions was maintained by substituting sucrose for the main electrolyte to avoid osmotic effects (Zimmerberg et al., 1990; Rayner et al., 1992; Starkus et al., 1995).

The main result is illustrated by Fig. 2 A. After excision of the patch into a solution of $S = 324$ mM, gating currents were recorded. Subsequently, the patch was locally perfused with a solution of lowered *S*. The amount of the charge was calculated from integration of the gating current at potentials where the charge has saturated. Exposure to a solution of $S = 24$ mM reduces the charge by $8.7 \pm 3.5\%$ ($n = 6$). This reduction happens with little shift in the voltage dependence of charge movement (Fig. 2 C). The fact that the reduction of *S* does not shift the $Q(V)$ curve suggests that the net surface charge in the intracellular part of *Shaker* channels is very small.

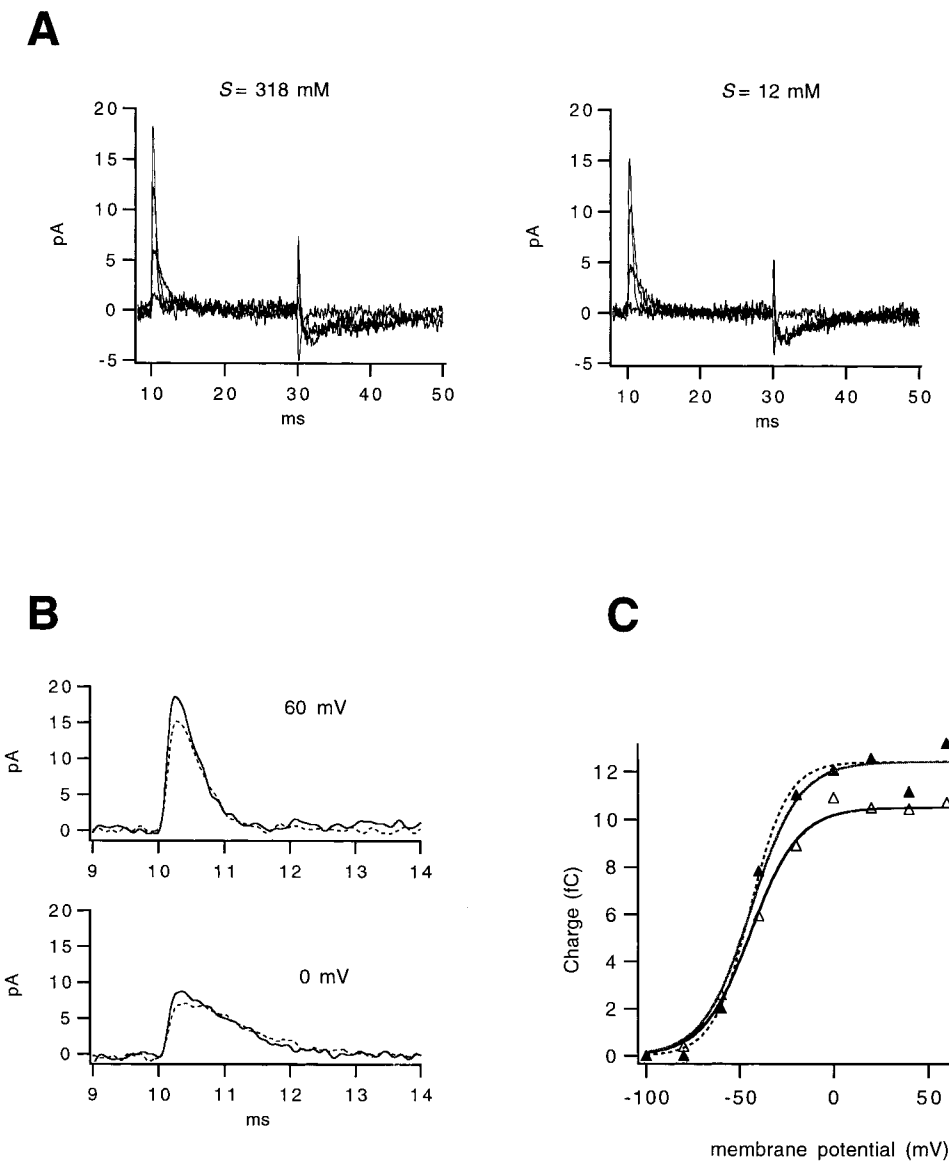

FIGURE 3. Effects of low ionic strength solutions (12 mM) on the gating currents of *Shaker*. (A) Gating current traces before and after perfusion of the intracellular side of a patch for depolarizations from −30 to 60 mV from a holding potential of −90 mV. (Left) Internal solution is control Cs (S = 318 mM); (right) S = 12 mM. The spikes of the current at the beginning of the OFF gating current trace are produced by an artifact of leak subtraction. (B) Traces at the indicated potential from the same patch in A before (continuous line) and after (dotted line) perfusion with the low ionic strength solution in an expanded time scale. (C) The full $Q(V)$ relationship. Open symbols are the charge in low ionic strength and closed symbols are the control. A reduction of ~16% in the charge is apparent from this patch. The continuous curves are fits to a Boltzmann function. The dotted curve is the scaled fit to the low ionic strength data. The parameters of the fits are as follows. For S = 318: Q_{max}= 12.4 fC, $V_{0.5}$= −4.4 mV, and q_g= 1.7 e_o. For S = 12 mM: Q_{max}= 10.5 fC, $V_{0.5}$= −44 mV, and q_g= 1.9 e_o.

This reduction of the amount of charge, although modest, is larger than the 1.7% decrease that would be expected from charge movement within a simple planar membrane (Fig. 1). To try to understand this reduction better, the gating current noise was measured from an ensemble of gating currents at high and low *S*. The variance is reduced by ~20% by the reduction of *S* (Fig. 2 B). In the limit of large depolarizations, the mean gating current and its variance are functions of the gating charge as follows:

$$I_g(t) = \nu q$$
$$\sigma^2(t) = 2B\nu q^2 = 2BqI_g(t), \quad (8)$$

where q is the elementary gating charge, n is the rate of charge movement, and B is the bandwidth of the recording (Conti and Stühmer, 1989; Crouzy and Sigworth, 1993). The fitted values of q from the mean and variance time courses in Fig. 2 are 1.0 e_o for S = 318 mM and 0.8 e_o for S = 24 mM. This result is consistent with the idea that the effect of low S is to diminish the size of the individual gating charge shots.

A further reduction of S to 12 mM produces the larger reduction of the total charge of 16.1 ± 2.9% (n = 4), and still no significant shift in the $Q(V)$ relationship is detected. Fig. 3 shows data from one such experiment. These experiments at a lower S were carried out with either NMDG-aspartate or CsCl as the cation-anion pair without observing any major difference.

It is conceivable that the reduction in the size of the gating current arises from a reduction in the number of functional channels or through immobilization of the channel gating mechanism. To test for these possibilities, the influence of a low S on the ionic currents of

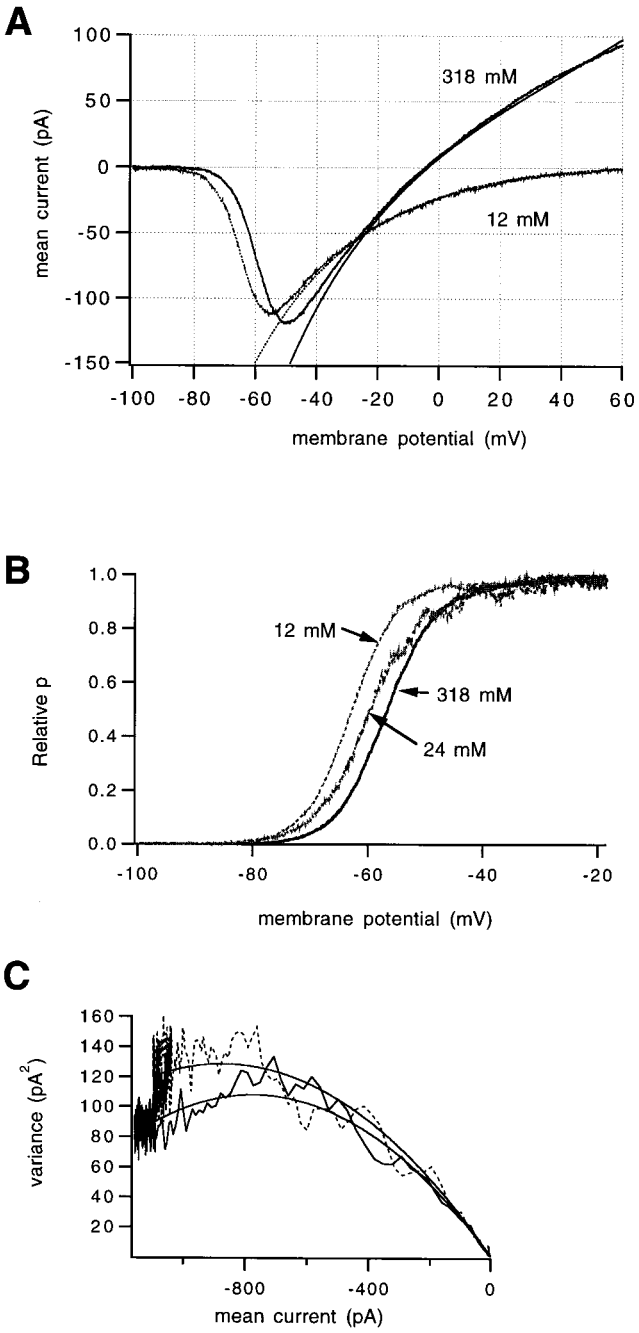

FIGURE 4. Ionic strength effects on ionic currents of *Shaker*. (A) $I(V)$ relationships obtained from ramps of voltage (0.32 mV/ms) using S = 318 K-Asp intracellular K^+ solution and switching to S = 12 mM intracellular solution. The external solution is pipet K. The continuous curves superimposed in the $I(V)$ curves are fits to a open channel $I(V)$ curve derived from a single barrier permeation model according to

$$I(V) = G_a[[K]_i e^{(-(1-\delta)ze_oV/(kT))} - [K]_o e^{(\delta ze_oV/kT)}],$$

where $[K]_o$ and $[K]_i$ are the extracellular and intracellular potassium concentrations, respectively, δ is the electrical distance, and z is the valence; e_o, k, and T have their usual meanings. G_a has units of nanoamperes per millimolar. The values used in the fit are for S = 318 mM, δ = 0.7, and G_a = 0.37 nA/mM. For S = 12 mM, δ = 0.7 and G_a = 0.23 nA/mM. The value of z remained constant at unity. (B) The relative open probability as a function of voltage at three different ionic strengths. The continuous traces are obtained from the ramps in A by dividing by the open channel $I(V)$ function. Boltzmann fits show that the lowest ionic strength solution (12 mM) produces a 10-mV shift in the hyperpolarizing direction. The shift at 24 mM is 6 mV. (C) Nonstationary noise analysis of currents at −20 mV recorded at 8 kHz bandwidth. The effect of the lower ionic strength is to increase the single channel conductance by a small factor that accounts for the increased variance, while the change in the open probability and the number of channels is also small. The estimated values from a fitted parabola (continuous curves) are as follows: at 318 mM, i = −0.24, pA, N = 5,624, and p_{max} = 0.81. At 12 mM, i = −0.3 pA, N = 5,605, and p_{max} = 0.67.

conducting channels was determined. Experiments were carried out in which the intracellular face of inside-out patches was perfused with low S solution, while the inward current carried by potassium was recorded (Fig. 4). Under these conditions, noise analysis was used to determine the open probability and the number of channels in the patch.

The changes observed in the shape of the current–voltage relationship in low S are consistent with a change in the driving force being the main difference. With the S = 12 mM (NMDG) internal solutions, the outward current disappears, and the reversal potential shifts by >60 mV. The nonlinear $I(V)$ relationship in symmetrical K^+ concentrations has been observed previously (Heginbotham and MacKinnon, 1993), and we account for it by using a simple permeation model having a single energy barrier (see Fig. 4 legend). The other main effect of a low S is that the activation seems to be shifted in the hyperpolarizing direction by ~10 mV at S = 12 mM and 6 mV at S = 24 mM (Fig. 4 B).

The nonstationary variance was also determined from multiple pulsed sweeps to a voltage where the function $p(V)$ is saturated (Fig. 4 C). This provides estimates of the open probability and the number of channels. It is seen that by lowering S to 24 or 12 mM, the estimated number of channels diminishes by <1% (from 5,624 to 5,605 in this experiment). This result confirms that the charge reduction observed in gating currents is not a simple result of fewer channels contributing to the recording. The maximum open probability is also changed very little, from 0.81 at 324 mM to 0.67 at 12 mM.

Finally, to test if the use of sucrose solutions to reduce S has a specific effect on charge movement, mannitol-containing solutions were used. Gating currents in low S solutions (12 mM) prepared with mannitol also display a reduction of the gating current comparable to that observed at the same S with sucrose solutions. Gating charge is reduced by 17.5 ± 4.3% (n = 2). No significant shift in the $Q(V)$ curve or the gating current kinetics was observed (Fig. 5). This supports the

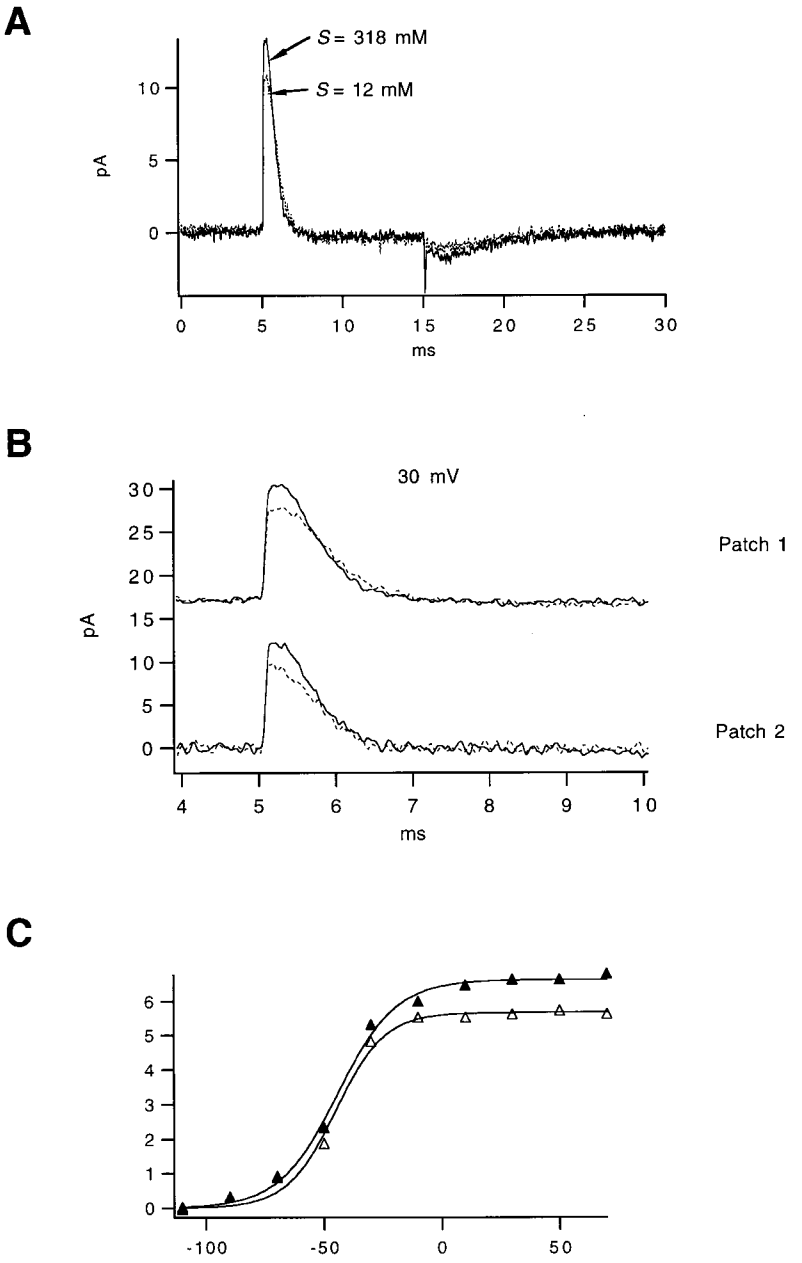

FIGURE 5. Effects of mannitol-containing low ionic strength solutions (12 mM) on the gating charge movement in *Shaker*. (A) Gating current traces before and after perfusion of the intracellular side of a patch for depolarizations from –90 to 30 mV. (Continuous trace) 318 mM(CsCl); and (dotted trace) 12 mM CsCl, with mannitol substituted for sucrose. (B) Two different patches at 30 mV in control solution (continuous line) and after (dotted line) perfusion with the S = 12 mM mannitol solution in an expanded time scale. (C) The full $Q(V)$ relationship for the top patch in B. Open triangles are the charge in S = 12 mM, and closed triangles are the control in S = 318 mM. A reduction of 14.5% in the charge is apparent from this patch. The continuous curves are fits to a Boltzmann function. The parameters of the fit are as follows: at 12 mM, Q_{max}= 5.7 fC, $V_{0.5}$ = −45.1 mV, and q_g = 2.4 e_o. At 318 mM, Q_{max} = 6.6 fC, $V_{0.5}$ = −44.3 mV, and q_g = 2.0 e_o.

idea that the effects are produced by low S and not by specific effects of the osmoticant.

It has been shown that the absence of permeant ions in the extracellular side of the pore of *Shaker* K^+ channels accelerates the rate of C-type inactivation (Baukrowitz and Yellen, 1996). This process is accompanied by an immobilization of charge in response to prolonged depolarization (Olcese et al., 1997). To test for the possibility that C-type inactivation may be responsible for the reduced charge observed here, we examined the charge movement as a function of time both in the high S solution and after perfusion with the low S solution. Fig. 6 shows an experiment in which the charge was monitored for ~40 s in a solution of S = 318 mM and also in S = 24 mM (Fig. 6, A and B). The charge remains constant for the duration of the recordings (Fig. 6 C). This indicates that there is not an appreciable degree of accumulation of slow inactivation or rundown.

Fig. 6 D also shows that the effects of low ionic strength are almost fully reversible. After exposure to S = 24 mM and return to high S solution, the charge recovers to within 98% of that of the control. In two additional patches, the recovery was within 97% and, in three more, it was within 95% of the control. These experiments indicate that charge reduction seems not to be a product of cumulative slow inactivation, and combined with the fact that the open probability and the number of functional channels in the patch is changed

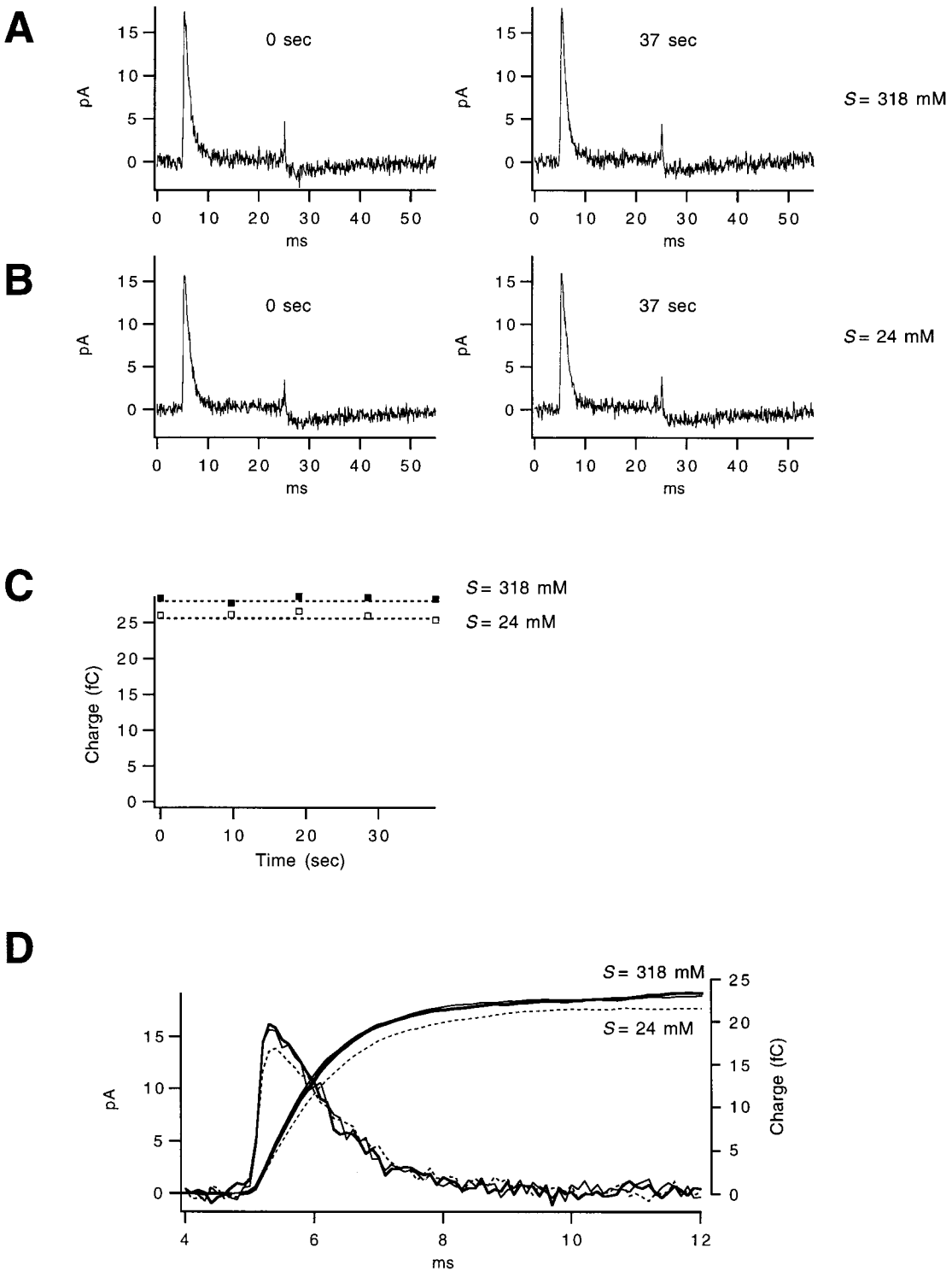

FIGURE 6. Tests for possible charge immobilization produced by slow inactivation of *Shaker* channels. (A and B) Representative average gating currents obtained from 10 sweeps for depolarization from –90 to 0 mV. The pulse interval was 200 ms for averaging, and an average was acquired every 9 s. The high *S* solution in A was intracellular control NMDG and the low *S* solution in B was intracellular 24 (Table I). (C) The ON gating charge plotted as a function of time for the patch in A and B. The total observation time was 37 s in each solution. The charge in either solution remains constant for the duration of the patch life, indicating that at least in this period there is no detectable charge immobilization. (D) Reversibility of the *S* effect. Gating current and its time integral are shown from a different patch. The thick trace is the control; the dotted trace is the gating current or charge in the low *S* solution (24 mM); and the thin trace is the gating current or charge after return to the high *S* solution 4.5 min later. In this particular experiment, the charge recovers to 98% of the control.

very little by a low *S*, argue in favor of the interpretation that the reduction of the gating charge is caused by the reduction of intracellular ionic strength only.

Extracellular Effects

We first attempted to measure the effect of lowering *S* of the extracellular solution in outside-out patches, but these were not stable in low *S* solutions, and the integration of gating currents was unreliable. For this reason, we decided to use the cut-open oocyte technique (Taglialatela et al., 1992). In preliminary experiments using perfusion of the upper chamber with low *S* solutions, we observed a very large reduction (55%) of the gating currents. This could arise from different patterns of current flow at the boundary between the top and guard chambers during perfusion of the top chamber with low *S* solutions.

For this reason, we decided to perfuse both the guard and top chambers. Simultaneous perfusion of the chambers with low *S* solutions resulted in only a small decrease in charge movement. To be certain that this decrease is not artifactual, we also tested the effect of low *S* on whole oocytes using two-microelectrode voltage clamp. Lowering the external *S* to 28 or 16 mM was seen to produce a very modest change in the size of the gating currents. The reduction of the charge is ~2.2% at 28 mM. This effect is seen in both two-electrode voltage clamp recordings and in cut-open clamp recordings (Fig. 7). A larger reduction of *S* to 16 mM produces a reduction in the charge of 3.5%. A reduction of extracellular *S* produces only a small shift in the voltage dependence of charge movement: the average shift at $S =$ 16 mM is <5 mV in the depolarizing direction.

A very interesting observation in the extracellular ef-

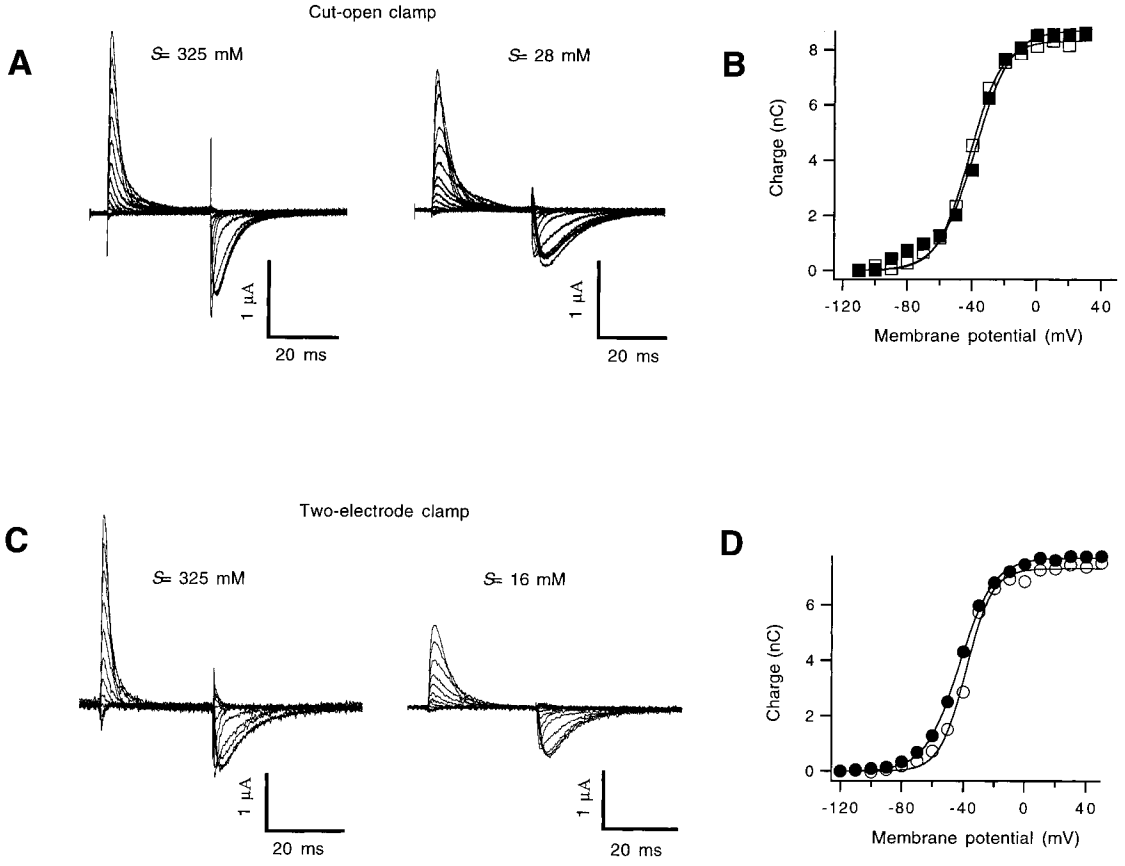

FIGURE 7. Extracellular effect of low ionic strength solutions on charge movement. (A) Gating current traces from the cut-open oocyte clamp in extracellular control solution $S = 325$ mM are on the left. The right panel shows currents at $S = 28$ mM. (B) The corresponding $Q(V)$ relationships. The parameters of the fitted Boltzmann function (continuous curves) are at $S = 28$ mM, $Q_{max} = 8.7$ nC, $V_{0.5} = -38.6$ mV, and $q_g = 2.3$ e_o. At $S = 325$ mM, $Q_{max} = 8.3$ nC, $V_{0.5} = -41.8$ mV, and $q_g = 2.5$ e_o. The maximum charge is reduced 4.2%. Closed symbols represent the control charge, and open symbols are the charge in low ionic strength. (C) Gating currents from a different oocyte recorded using the two-microelectrode voltage clamp. The low ionic strength solution is extracellular 16 mM. (D) $Q(V)$ relationships of the experiment in C. Open circles correspond to the charge in low ionic strength. The following are parameters of the fitted Boltzmann function at $S = 16$ mM: $Q_{max} = 7.7$ nC, $V_{0.5} = -38.2$ mV, and $q_g = 2.9$ e_o. At $S = 325$ mM: $Q_{max} = 7.7$ nC, $V_{0.5} = -42.5$ mV, $q_g = 2.2$ e_o. The charge is reduced by 5.2% in the $S = 16$ mM solution.

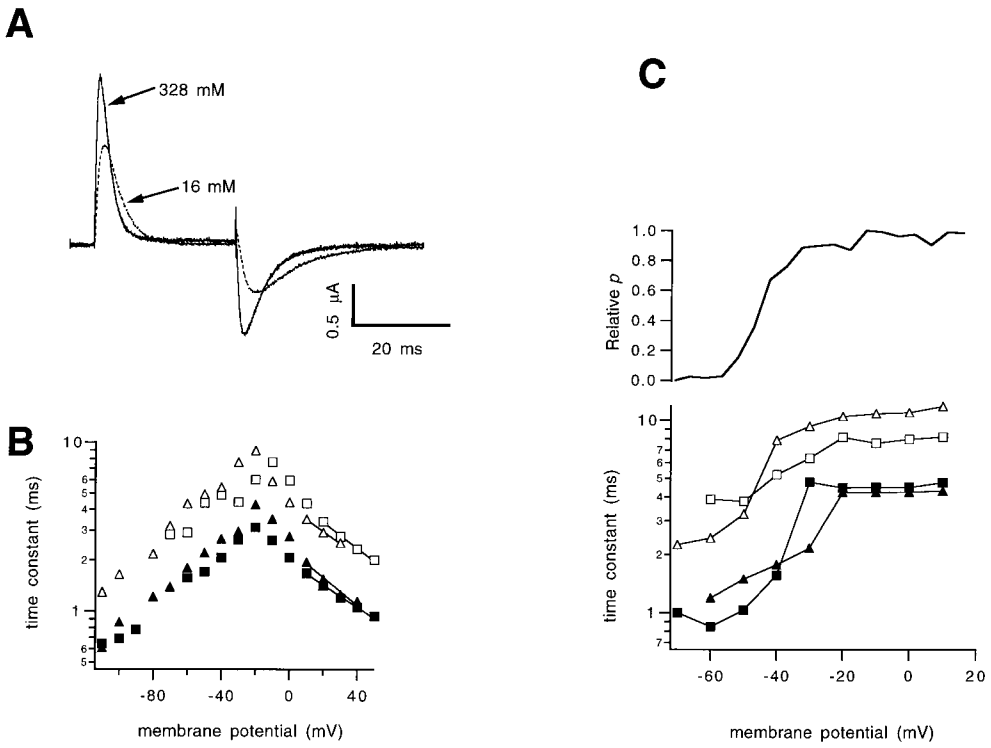

FIGURE 8. Comparison of gating current kinetics at high and low extracellular ionic strength. (A) Gating currents at 0 mV obtained with the cut-open voltage clamp. The faster trace was obtained at S = 325 mM and the slower trace corresponds to S = 16 mM. It is evident that both the ON and OFF kinetics are slowed down. (B) Comparison of the time constants of current decay, τ_{on}. ON gating currents were fitted to a single exponential function, and the time constant was plotted as a function of voltage. Open symbols are the data points at low ionic strength (S = 16 mM). Closed symbols are the data at high ionic strength (S = 325 mM). Squares correspond to data obtained with the two-microelectrode voltage clamp, and triangles correspond to cut-open voltage clamp. Solid lines correspond to fits of the most depolarized points to the function: $\tau_{on}(V) = \tau_{on}(0) \cdot \exp(-q_{on}V/kT)$. The values of q_{on} are as follows: (open triangles) 0.41 e_o; (open squares) 0.44 e_o; (closed triangles) 0.47 e_o; and (closed squares) 0.37 e_o. (C) Time constant of decay $\tau_{OFF}(V)$ for OFF gating currents. A single exponential was fitted to the decay phase of the current and is plotted as a function of the potential during the activation pulse. The upper panel in the figure is the relative open probability $p(V)$ as a function of voltage, obtained from conducting channels (ShΔ) recorded from a cell-attached patch in low external K^+ solution with high S (295 mM). Note that the function $\tau_{OFF}(V)$ has a similar voltage dependence to $p(V)$.

fects of low S is that gating current kinetics are slowed considerably. Fig. 8 A shows gating current traces at 0 mV obtained before and after lowering the S of the extracellular solution. Both ON and OFF gating currents are slowed. The slowing of ON gating currents is seen in Fig. 8 B as an approximately twofold increase in τ_{ON} at all voltages. The OFF gating currents are slowed down by a similar amount (Fig. 8 C). The voltage dependence of the OFF gating currents is consistent with that of the activation of macroscopic currents in the same extracellular solutions (high S). At membrane potentials where the channels begin to open, the OFF gating currents become slower because of the slow rate of exit from the open state (Zagotta et al., 1994; Schoppa and Sigworth, 1998). The slowing of both ON and OFF gating currents by a similar amount is consistent with the absence of a shift in the equilibrium distribution of charge movement.

These effects of a lowered S are not explained by a simple voltage shift of the kinetics, as predicted by electrostatic screening of surface charge. In experiments involving changes in external pH, Campbell and Hahin (1984) observed a similar slowing of kinetics of Na^+ channel gating currents at low pH that was not a simple shift in the voltage axis. Clearly, not all ionic strength effects are mediated by the screening of fixed charges.

Electrostatic Calculations

Is it possible to give a mechanistic interpretation to the reduction of charge observed in low S in the intracellular part of the channel? In Eqs. 1–4, we have presented the argument that the degree of coupling to the membrane potential and the gating charge is measured as the gating current. A reduction in S would be expected to reduce coupling by affecting the local potential that the gating charges sense. To interpret the experimental results within this formalism, we performed a calculation to try to account for the effects of S on gating currents in terms of a gating pore. For this purpose, the linearized Poisson-Boltzmann equation was solved in cylindrical coordinates using a finite difference algorithm to investigate the dependence of the local potential on the geometry of the membrane.

In this scheme, it is possible to set up a membrane surrounded by high dielectric constant regions that simulate the intracellular and extracellular solutions. Also a cavity of arbitrary shape and molecular dimensions can be made in the membrane (Fig. 9 A). This is meant to simulate the gating pore. By examining the local potential in this model pore, one can get an idea of the expected magnitude in the change of gating charge as a function of S and the shape and dimensions

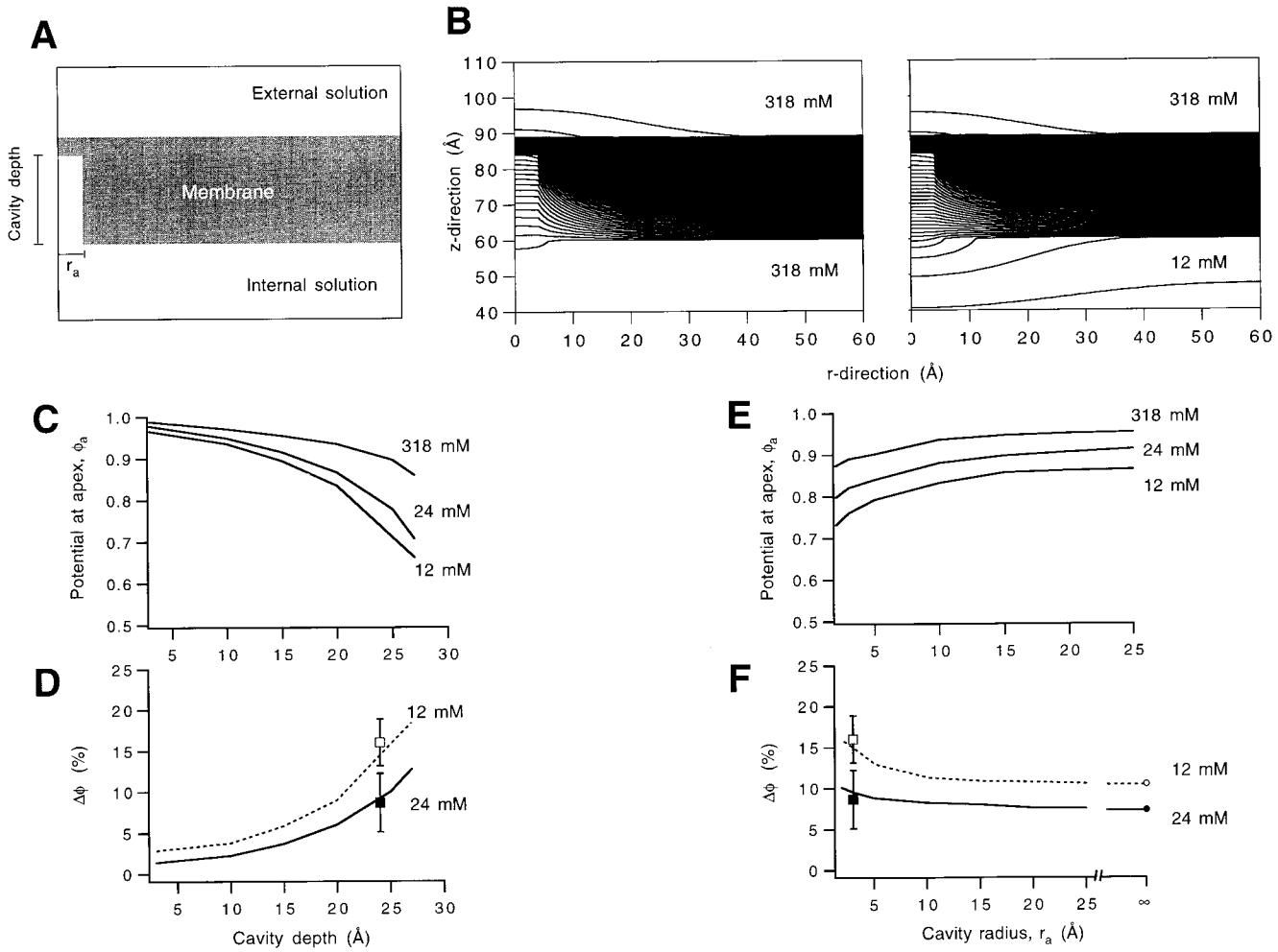

FIGURE 9. Numerical solutions of the linearized Poisson-Boltzmann equation in cylindrical coordinates for a cylindrical cavity in the membrane. (A) Schematic representation of the geometry used for the calculations. The grid dimensions were 0.5 Å in the r (radial) direction and 0.5 Å in the z direction. The membrane thickness was 30 Å. (B, left) potential distribution at high (318 mM) internal ionic strength. Isopotential lines were plotted at intervals of $0.006V$, where V is the imposed membrane potential. (B, right) Potential distribution with low internal ionic strength (12 mM). The values of S are indicated in each panel. (C) Dependence of the apex potential (ϕ_a) on the depth of a cylindrical cavity of radius $r_a = 3$ Å. The calculation was run at the following depths: 3, 5, 10, 15, 20, 25, and 27 Å. Notice that the largest reductions of ϕ_a are obtained with a deep cavity and low S. (D) Continuous lines are the absolute potential reduction calculated as $\Delta\phi = \phi_a(318) - \phi_a(S)$, where $\phi_a(318)$ is the value of ϕ_a at 318 mM and $\phi_a(S)$ is ϕ_a at $S = 24$ or 12 mM. The data points correspond to the mean ± SEM of the experimentally measured reductions of gating currents plotted arbitrarily at a depth of 24 Å. (E) Potential at the apex ϕ_a of a 25-Å-deep cavity as a function of the radius r_a at the indicated values of S. (F) The potential change $\Delta\phi$ calculated from the data in E. The continuous line represents the potential reduction $\Delta\phi$ with $S = 24$ mM, and the dotted line is $\Delta\phi$ at $S = 12$ mM. The data points are plotted at an arbitrary radius of 3 Å. The small circles represent the asymptotic value of the potential reduction for an infinite membrane of 5 Å thickness at the indicated values of S, which was obtained with the analytical solution presented in Eq. 7.

of the cavity. The dielectric constant is set to a value of 80 in solution and 2 in the membrane, and it is initially assumed that the dielectric constant in the cavity is the same as that of the bulk solution. The value of κ in the cavity is also set equal to its value in the adjacent solution, while κ is zero elsewhere in the membrane.

Fig. 9 B shows an example of such a calculation for the cylindrical cavity. Isopotential lines are shown in a slice through the center of the membrane cavity system. The calculation was done with a cavity of 3-Å radius (r_a) and 25-Å depth in a membrane of 30 Å thickness. The intracellular value of S was changed from its high value of 318 mM (Debye length $\kappa^{-1} = 7.6$ Å) to values of 24 mM ($\kappa^{-1} = 21$ Å) and 12 mM ($\kappa^{-1} = 30$ Å). The extracellular value of S remained fixed at 318 mM. The effect that the cavity has on the membrane potential distribution is to increase the fraction of the potential that falls in the solution and in consequence, reduce the potential measured at the apex of the cavity (ϕ_a). Assuming that the gating charge moves between the cavity's apex and the external surface, this produces a reduced gating charge because the fraction of

membrane potential that the gating charge traverses is now diminished and the difference in $\delta_{i\lambda}$ (Eq. 1) between resting and activated states is also reduced. As *S* is lowered in the intracellular space, ϕ_a is further reduced. This is seen by an increase in the number of isopotential lines in the intracellular side (Fig. 9 B, right).

At a given pair of intra- and extracellular *S* values, the depth or the diameter of the cylindrical cavity was varied while maintaining the other constant at a given value. Fig. 9 C shows the value of ϕ_a in the 3-Å radius cylindrical cavity, as a function of the depth of the cavity at the three indicated values of *S*. The same data are transformed in Fig. 9 D to give the fractional reduction of potential produced upon going from $S = 318$ mM to 24 mM and 12 mM. This value, $\Delta\phi$, is the difference of ϕ_a at two values of *S*. The data points with the error bars are the experimentally measured charge reductions produced by changing intracellular ionic strength, and plotted arbitrarily at the depth value of 24 Å to fit the calculated curves.

The calculation was also performed in a cavity of depth 25 Å for various values of r_a. The changes in r_a have only a moderate effect on ϕ_a, as shown in Fig. 9 E. The reduction of ϕ_a is more pronounced with a smaller radius, but for both $S = 12$ mM and 24 mM at radii >6 Å, the reduction rapidly approaches the asymptotic value given by an infinite, thin membrane. The experimental data seem to be consistent with a cavity of a radius of 3 Å and a depth of 25 Å out of the total 30-Å membrane thickness. (Fig. 9 F). However, for a deeper cavity, the larger radius would also satisfy the data. In general, it is seen that the cavity must be narrow and deep to produce the observed $\Delta\phi$ values.

The same kind of numeric calculation was performed using a truncated conical cavity. This geometry has an added parameter, which is the radius r_m at the mouth of the cavity, and is presented schematically in Fig. 10 A. The value of r_a was left constant at 3 Å to facilitate comparisons with other geometries, and the effect of varying the depth of the cavity with radii $r_m = 3$, 6, and 10 Å was investigated. At a constant r_m, the effects on the potential are qualitatively similar to that observed in the cylindrical cavity, i.e., ϕ_a diminishes as the cavity becomes deeper and is also diminished at a lowered *S*. As the value of r_m is made larger, the depth that is necessary to account for experimental values is increased. The mouth aperture of the cone has a progressively more important effect as the cone becomes deeper. The data are best approximated with a cone of $r_m = 10$ Å and a depth of the cavity of 28 Å (Fig. 10 A). Overall, the conical cavity produces smaller changes in ϕ_a than the cylindrical cavity, and it is necessary to have a deeper cone compared with a cylinder to account for the experimental observations. It seems that the progressively increasing radius from r_a to r_m in the truncated cone allows for less crowding of the electrical potential inside the cavity.

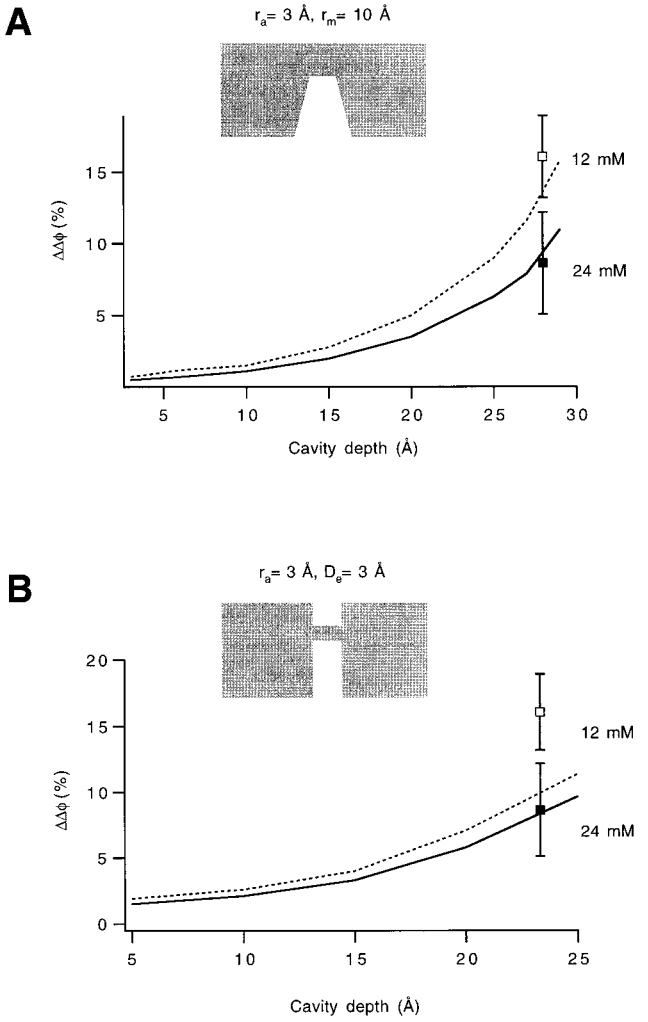

FIGURE 10. Numerical solutions of the linearized Poisson-Boltzmann equation for two different geometries. (A) Truncated conical cavity. The membrane thickness was 30 Å, and the cone radii were fixed at $r_a = 3$ Å and $r_m = 10$ Å as the cavity depth was varied. The top diagram is a schematic representation of the geometry. The potential difference in the short slab of membrane was calculated as $\Delta\phi_m = \phi_a - \phi_e$, where ϕ_a is the potential at the apex of the internal cavity and ϕ_e is the potential at the external surface of the membrane axially opposite to ϕ_a. The effect of changing *S* was calculated as $\Delta\Delta\phi = \Delta\phi_m(318) - \Delta\phi_m(S)$. (B) Double cylindrical cavity. The radii $r_a = r_m$ of both cavities were 3 Å, and the depth of the external cavity was $D_e = 3$ Å. The extracellular side and cavity have a constant high ionic strength of 318 mM. The reduction of potential $\Delta\Delta\phi$ was calculated (as in A) as a function of depth of the internal cavity. The calculation was done at depths 5, 10, 15, 20, and 25 Å. The symbols correspond to the experimental reductions plotted at 23 Å.

Explaining Extracellular and Intracellular Effects

Since we have observed some charge reduction while reducing *S* in the extracellular face, we attempted to explain the effects of both intracellular and extracellu-

lar reductions of S with a calculation using a membrane with both internal and external cavities. Since the extracellular effects are smaller, we used a small cavity for the external face. At a given value of S, the potential reduction was now calculated as the difference between the potential at the apex of the internal cavity ϕ_a and the potential at the bottom of the external cavity ϕ_e. This difference is called $\Delta\phi_m$ and represents the effective membrane potential. The effect of going from a high to a low value of S is called $\Delta\Delta\phi$ and is calculated as the difference $\Delta\Delta\phi = \Delta\phi_m(318) - \Delta\phi_m(S)$.

As in previous calculations, the depth of the internal cavity D_i was varied while keeping a fixed value of r_a = 3 Å and a fixed value of the external cavity depth D_e = 3 Å (Fig. 10 B). The results of these calculations are qualitatively similar to those obtained with the internal cavity and the planar external face, but the reduction of potential $\Delta\Delta\phi$ produced by S = 12 mM is smaller than in the other geometries. If the calculation is repeated with an external cavity depth of 5 Å, the values of $\Delta\Delta\phi$ are even smaller. To try to explain the experimental results with this geometry, the value of D_i has to be 23 Å, but the reduction in gating charge produced by lowering S to 12 mM is underestimated (Fig. 10 B). With an internal cavity depth D_i = 23 Å and an external cavity depth D_e = 3 Å, and keeping the value of internal S at 325, the values of $\Delta\Delta\phi$ produced by changing external S are 2.2% at S = 28 mM and 2.6% at S = 16 mM. The experimentally observed reductions of the gating charge with the reduction of extracellular S are 2.3 ± 1.4% for S = 28 mM and 3.2 ± 1.2% for S = 16 mM. Nevertheless, it seems that if there is an external cavity, as in our double cavity system, this has to be much smaller than the internal cavity and the space between the external and internal cavities has to be a very small slab of ~4 Å thickness.

Effects of Model Parameters

It is likely that the dielectric constant of water in a pore-like cavity is different from that of bulk water. Sansom et al. (1997) have shown that the helix dipoles of a helix bundle can produce polarization saturation of water molecules, effectively reducing the value of ε. This effect may be smaller in anti-parallel helix bundles, as those expected to form the walls of the gating pore. Nevertheless, we were interested in testing the effect of having a smaller ε in the internal cavity and set up a membrane system with truncated conical external and internal cavities in which the value of ε in the internal cavity is 30. The value of κ in the internal cavity is changed accordingly (Eq. 6). The potential at the apex of the internal cavity ϕ_a and on the base of the external cavity ϕ_e are reduced by the low value of ε. The potential in the membrane more readily penetrates the internal cavity, and the reduction of S produces larger effects in the values of $\Delta\phi_m$. Fig. 11 B shows the dependence of $\Delta\Delta\phi$ on the depth of a cylindrical double cavity of radius r_a = 3 Å. The main effect of having a reduced dielectric constant in the internal cavity is that the percent reductions of the effective membrane potential $\Delta\Delta\phi$ are larger than in the same geometry with ε = 80. As was noted previously (Fig. 10 B), having an external as well as an internal cavity in the membrane system produced smaller reductions of a membrane potential. Now with a reduced ε, the system better accounts for the experimental observations. Using the truncated conical double cavities, the measured reductions of gating charge produced by reducing S, either internally or externally, can be explained simultaneously by having an external cavity of depth D_e = 3 Å and an internal cavity of depth D_i = 20 Å, with radius r_a = 3 Å and internal mouth opening r_m = 10 Å (Fig. 11 C).

It seems that allowing for a reduced dielectric constant of 30, the double cavity system with the truncated cones provides a good description of both the intracellular and extracellular reductions of charge. The use of ε = 30 for the solution in the cavity seems reasonable in view of the calculations of Sansom et al. (1997), and also allows for a larger cavity with a minimum radius r_a = 3 Å, which is in agreement with the ability of large MTS reagents to modify S4 residues. The dimensions of the external and internal cavities reduce the region of membrane potential focusing to a septum of ~7 Å thickness. In the normal high S solutions (~300 mM), the drop of potential across the septum in Fig. 11 C is 91% of the full membrane potential.

We have used 30 Å as the thickness of the hydrophobic core of the bilayer and the height of the channel protein. This is close to the ~35 Å height of the KcsA channel (Doyle et al., 1998) and 26 Å for gramicidin (Roux and Karplus, 1991). To investigate the effect of the (unknown) size of the *Shaker* channel, we performed calculations like those shown in Fig. 11 A, but used a membrane–channel thickness of 40 Å. As can be seen in Fig. 11 D, the effects of a deep cavity are qualitatively similar to those of the 30-Å system, but the cavity has to be as deep as 25 Å to account for the experimental observations. This means that the effect of increasing the thickness of the membrane–channel system is to scale up the dimensions of the cavity. In this case, the expected thickness of the septum increases from 7 to 13 Å.

Another issue is related to the value of the dielectric constant of the protein, ε_p. Molecular dynamics calculations in soluble proteins have suggested that the value of ε_p should be larger than that of the lipid bilayer. Antosiewicz et al. (1996) have shown that in calculating the pK_a of titrable groups of proteins in aqueous solutions, values for ε_p of 4–8, and perhaps as high as 20 provide better agreement of the MD calculation with actual data. However, the issue of the value of ε_p is an open one and, recently, more elaborate calculations

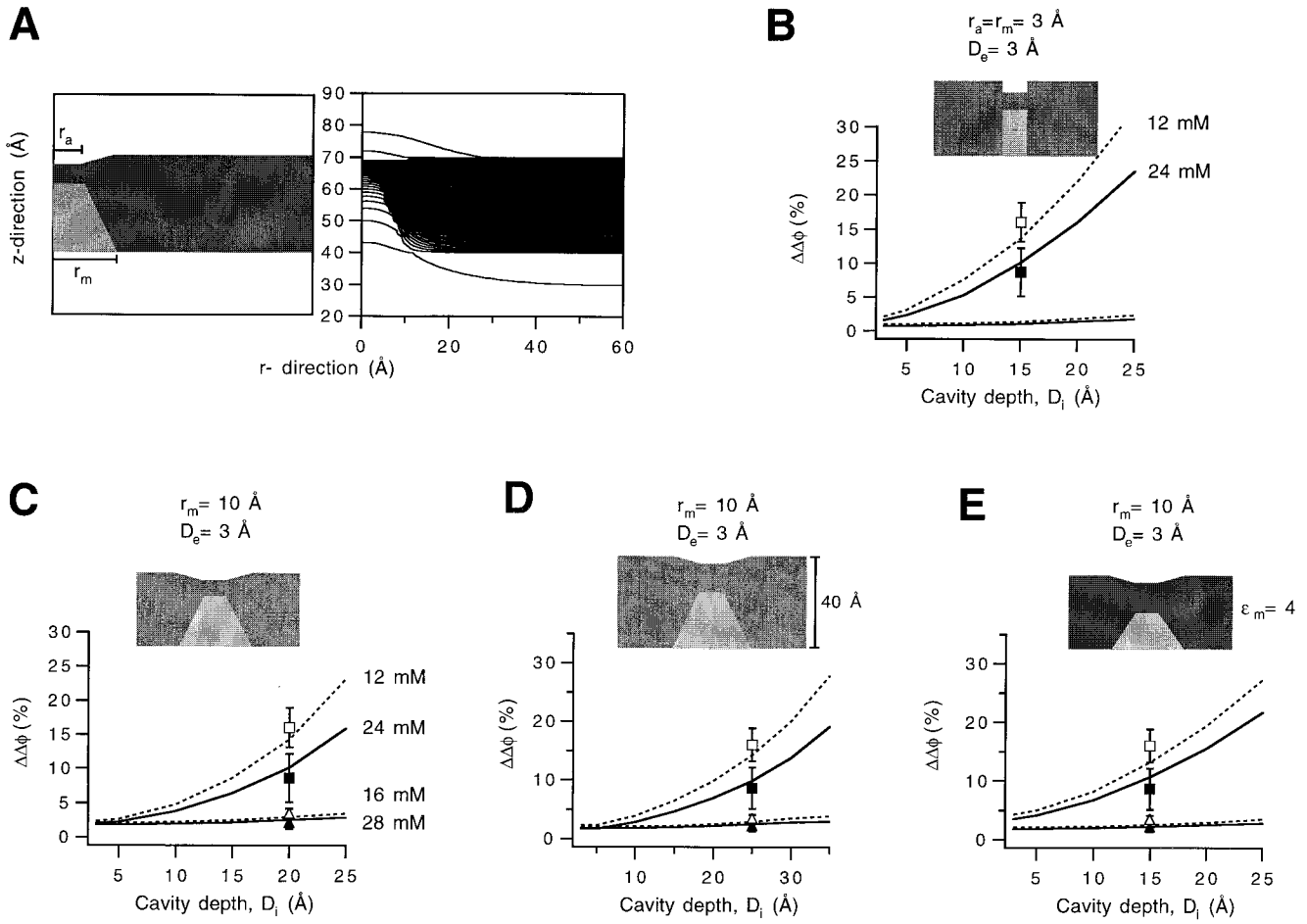

FIGURE 11. Calculated effects of S in the double cavity system with low dielectric constant ($\varepsilon = 30$) in the internal cavity. (A) The radius r_a is the same for the external and internal cavity, and the mouth radius r_m was varied. The geometry of the system is shown in each panel. The internal cavity depth is D_i, and the external cavity depth is D_e. (B) Variation of the potential difference as a function of D_i in the double cylinder. The internal cavity has $\varepsilon = 30$. The function $\Delta\Delta\phi$ is calculated as $\Delta\Delta\phi = [\phi_a(318) - \phi_e(318)] - [\phi_a(S) - \phi_e(S)]$, where ϕ_a is the potential at the apex of the internal cavity and ϕ_e is the potential at the base of the external cavity. Traces are $\Delta\Delta\phi$ as a function of D_i at S = 24 mM (continuous curve) and S = 12 mM (dotted curve). Open squares are the observed charge reduction for a change in internal S to 12 mM; and closed squares are the reduction in charge for a reduction of internal S to 24 mM. (C) Similar calculation as in B but using a truncated-cone double-cavity system with the dimensions indicated and r_a = 3 Å. The upper traces are values of $\Delta\Delta\phi$ as a function of D_i for internal changes of S. The continuous trace is the change in potential for a change of S to 24 mM; and the dotted curve is the change of potential for a change of S from 318 to 12 mM. The data points correspond to the experimental reductions of charge at the indicated value of S plotted at a depth value of 20 Å. The traces at the bottom of the panel are the potential changes $\Delta\Delta\phi$ induced by reducing the external value of S from 318 mM to 28 and 16 mM, while keeping internal S constant at 318 mM. In each case, the external cavity had a depth D_e = 3 Å. The triangles are the experimentally measured reductions of charge for extracellular reductions of S, which are indicated. (D) The thickness of the membrane has been increased to 40 Å. The calculation was performed as in C with r_a = 3 Å and the parameters indicated on each cartoon. The cavity was assigned a dielectric constant of 30, and the bulk extracellular and intracellular solutions had a value of 80. The depth of the membrane D_i was changed to the indicated values. The $\Delta\Delta\phi$ values plotted are the potential difference across the septum for changes of S from 318 to 24 mM (continuous line) or to 12 mM (dotted line). The external cavity was fixed at 3-Å depth. The values in the bottom of the panel correspond to the calculation for the extracellular effects of S for changes from 318 to 28 mM (continuous) or 16 mM (dotted), while keeping the internal value of S constant at 318 mM. The experimental reductions of charge as a function of S were plotted at a cavity depth of 25 Å. (E) Effect of increasing the dielectric constant of the channel-membrane system to 4. The thickness of the membrane was 30 Å. The dielectric constant of the cavity and bulk solutions were 30 and 80, respectively. Note that this configuration poorly predicts the observed experimental effects of S, although the effects of reducing S are qualitatively similar to those obtained with $\varepsilon = 2$. The best fit cavity becomes smaller with $\varepsilon = 4$ than with an $\varepsilon = 2$.

have shown that a value of $\varepsilon_p = 2$ is appropriate (Sheinerman et al., 2000). Fig. 11 E shows results from a calculation as in Fig. 11 C using an ε_p of 4 for the membrane–channel system with a thickness of 30 Å. As can be seen, the higher value of ε_p reduces the size of the cavity necessary to approximate the experimentally observed effects of S; a predicted difference between S = 24 mM and S = 12 mM become less marked. This can be explained because the higher value of ε_p produces less decay of potential across the protein septum.

Finally, we address an issue related to the calculation of the effects of ionic strength using LPB theory. It has been suggested that the use of the Poisson-Boltzmann formalism is inadequate in the vicinity of a dielectric boundary because of a strong repulsive force on ions close to it. In a recent Brownian dynamics study, Moy et al. (2000) have shown that within a few angstroms of a dielectric boundary there is a depletion of ions because of the repulsive reaction field. The repulsion increases as the charge squared and, therefore, is incorrectly described by a continuum of charge. To first order a small depletion of ions near a dielectric boundary is negligible in terms of ionic screening, because anions and cations are depleted equally; however, when the reaction potential exceeds the value of kT, the effects will be substantial. Consider a monovalent ion in a medium of dielectric constant ε_1 approaching a plane boundary with a medium of dielectric ε_2. Using the method of image charges, the energy from the reaction field is seen to be

$$U(r) = \frac{e_o^2(\varepsilon_1 - \varepsilon_2)}{16\pi r \varepsilon_o \varepsilon_1(\varepsilon_1 + \varepsilon_2)},$$

where r is the distance from the ion to the plane. Letting $\varepsilon_1 = 80$ and assuming ε_2 to be much smaller, $U(r)$ becomes equal to kT at ~1.7 Å. For $\varepsilon_1 = 30$ and $\varepsilon_2 = 2$, the critical distance becomes $r = 4.1$ Å. Because of this depletion of ions near the boundary, the effects we see in our calculations with cavity radii on the order of 3 Å are probably better modeled with a cavity radius a few angstroms larger. To account for the possibility of such an effect, we introduced an ion exclusion region, where the value of κ is set equal to zero, represented by a slab 4 Å thick surrounding the dielectric boundary in the internal cavity and 2 Å in the external cavity. Fig. 12 shows that the introduction of a cutoff region is equivalent to a reduction of the overall size of the cavity, so that the experimental data are approximated by a much deeper cavity. If the dielectric repulsion of ions in the cavity is significant, this means that the best cavity would have a radius $r_a = 6$ Å, a mouth radius $r_m = 14$ Å, and an internal depth $D_i = 24$ Å. In this case, the septum is reduced to a thickness of only 3 Å.

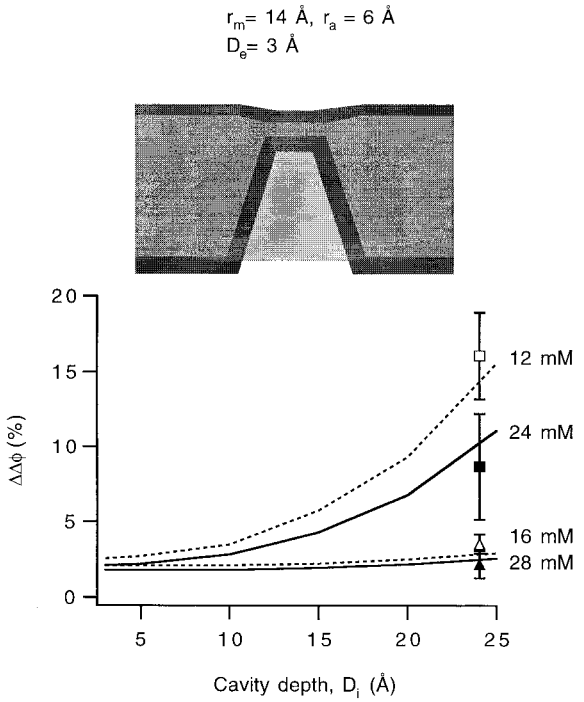

FIGURE 12. Effects of the inclusion of an ion depletion area in calculations using the conical geometry. Calculation with a bigger cone radius ($r_a = 6$ Å) and mouth radius ($r_m = 14$ Å) in the double-cone system. The external cavity depth is 3 Å. The dielectric constant of the membrane channel region is set at a value of 2, and the dielectric constant inside the cavity is set to a value of 30. The intracellular and extracellular data are plotted at 24 Å of internal cavity depth D_i. There is a cutoff region of 4 Å around the internal cavity, where the value of κ is set to zero to simulate the ion exclusion effect. The cutoff around the external cavity is set to 2 Å. This is illustrated in the cartoon, which is drawn to scale, by the darker band around the cavity and the membrane–solution boundaries.

DISCUSSION

In this paper, we have shown that reducing the ionic strength S causes small but reproducible reductions in the measured gating charge. An approximate 10-fold reduction of internal S produces an 8.7% reduction of gating charge. These effects continue at even lower values of S (Table II). A similar reduction of external S produces a much smaller reduction of 2.2%. It seems that the low S environment affects the local electric field and, thus, reduces the coupling between it and the intrinsic voltage-sensing charges, producing the observed reduction of the gating charge. The magnitude of the charge reduction is significantly larger than what is expected from a voltage sensor in a simple planar membrane (Table II). We have also shown that the $Q(V)$ curves have only small shifts in the presence of low S solutions, either on the intracellular or extracellular sides.

Surface Charge Effects

Previous studies have dealt with the effects of low S on ionic currents of voltage-activated Na^+ channels, inferring the existence of a negative surface charge in the intracellular and extracellular region of the channel and the surrounding membrane. This charge is thought to affect the gating and permeation properties by a simple electrostatic mechanism (Frankenhaeuser and Hodgkin, 1957; Chandler et al., 1965; Hille et al., 1975a,b; Cukierman, 1991).

TABLE II

Gating Charge Reduction at Low Ionic Strength

S	Percent planar expectation	Percent intracellular effect	Percent extracellular effect	*n*
24	1.7	8.7 ± 3.5		6
12	2.5	16.1 ± 2.9		4
28	1.5		2.3 ± 1.4	4
16	2.1		3.2 ± 1.2	3

Summary of the charge reductions produced by the reductions of internal or external ionic strength (*S*). The planar expectation is the reduction of potential for the indicated value of *S* calculated with Eq. 7 for a given pair of values of *S* as $\Delta\phi(318) - \Delta\phi(S)$ for the internal effects of *S;* and as $\Delta\phi(325) - \Delta\phi(S)$ for the external effects, where $\Delta\phi = \phi_a - \phi_e$. Here ϕ_a and ϕ_e are the potential at the apex of the internal cavity and at the base of the external cavity, respectively. The values of the reduction are the mean ± SEM The value *n* is the number of experiments.

Those experiments in which the effects of *S* were investigated relied on the measurement of ionic currents and their voltage dependence. In most cases, a shift in the voltage dependence was observed that was interpreted in terms of the surface potential theory, where the surface charge affects channel gating and permeation by setting up a bias potential that is superimposed on the membrane potential. If the fixed charge is negative, then a reduction of *S* is expected to produce a negative shift for changes at the extracellular medium and positive shifts for changes in the intracellular face. Because the shifts are taken to be the result of a bias potential, they should be of the same magnitude for steady-state and kinetic properties alike; but in most cases, this expectation has not been fulfilled. Several studies have shown that shifts of kinetic and steady-state parameters in the Na^+ channel are correlated with the occupancy of the pore and can be explained by a model that does not involve surface charge effects. Studies of the magnitude of the screening effects of calcium on Na^+ channels reached the conclusion that not only the surface charge effects of Ca^{2+} are small, but they also seem to be inconsistent with the canonical form of surface charge theory. It is possible to account for all the effects of Ca^{2+} by an occupancy model in which Ca^{2+} occupation of the pore is needed for the channel to close (Boccaccio et al., 1998; Armstrong, 1999).

In our experiments on *Shaker* potassium channels, ionic current activation is shifted in the hyperpolarizing direction upon reduction of internal *S,* by 6 mV at 24 mM and by 10 mV at 12 mM. The polarity of these shifts could be readily explained if the surface charge in the intracellular part of the channel is assumed to be positive and quite small. According to Gouy-Chapmann theory, it is possible to calculate an approximate charge density from the shifts of voltage dependence of 6.4×10^{-4} $e_o/Å^2$. Similarly, Elinder et al. (1998) have estimated an extracellular surface charge of -27×10^{-4} $e_o/Å^2$, which is roughly explained by the negatively charged amino acid residues on the external surface of the channel protein. Another explanation is that the removal of permeant ions from the intracellular space affects the equilibrium of the opening transition by an allosteric mechanism and is thus producing the shift. Our low *S* solutions had reduced K^+ concentrations. It is possible that absence of K^+ at the inside of the channel changes the energetics of the opening conformational change by a few *kT* units, which would be sufficient to produce the observed shift of voltage dependence.

Finally, it seems that the actions of divalent ions in *Shaker* gating currents are also inconsistent with the surface charge theory. Raising external Ca^{2+} does not modify charge movement, while the action of Ba^{2+} is explained by a selective acceleration of the rate of channel closing (Hurst et al., 1997). It is possible that the amount of fixed charge in potassium channels differs from that of their sodium counterparts and, in consequence, many of the effects previously attributed to surface charge screening in potassium channels, can be explained at least as well by gating effects of permeant or partially permeant ions. We conclude that surface charge effects on *Shaker* are small.

Ionic Strength Effects on Kinetics

We have shown that the extracellular reduction of *S* has a qualitatively and quantitatively different effect on gating currents than intracellular changes. The time constant of decay of ON and OFF gating currents is made slower in reduced extracellular *S*. The overall slowing of kinetics is inconsistent with a simple surface charge mechanism, but is similar to the effect of low pH on Na^+ channel gating currents (Campbell and Hahin, 1984).

It is possible that our low *S* solutions, having an increased viscosity, affect the gating kinetics by changing the energy barrier for one or multiple transitions. It has been shown that increased solution viscosity affects protein dynamics by a damping effect on the internal motion of the protein, affecting the energy barrier for a particular transition (Beece et al., 1980). In *Shaker* channels, exposure to hyperosmotic solutions slows the kinetics of activation of macroscopic currents, and the result has been interpreted in a similar way, as an increase of the energy barrier of one or multiple transitions (Starkus et al., 1995). The absence of a shift of the $Q(V)$ relationship is consistent with the observed slowing of both the ON and OFF gating currents by a similar amount. Also, the absence of a shift in the voltage axis is consistent with experiments in *Shaker* involving the effects of divalent cations (Hurst et al., 1997). In those experiments, the gating currents also did not change voltage dependence in the absence or presence

of divalent ions, which would be expected to produce surface charge screening effects.

A Cavity Explains Asymmetric Ionic Strength Effects

Reductions in intracellular ionic strength produce large reductions in the apparent gating charge. We have ascribed this effect to the potential drop in an intracellular aqueous cavity. However, it should be noted that a cavity is not required to explain the effect: a planar membrane that is sufficiently thin (say 5 Å) can also account for the intracellular effects, as shown in Fig. 9 E. The problem with a thin membrane (or equivalently, a very broad cavity) is that such a membrane would produce an equally large sensitivity to extracellular ionic strength changes, which is not observed. In the end, it is the asymmetry of the ionic strength effects that requires us to postulate a restricted cavity on the intracellular surface of the channel.

The estimated dimensions of the intracellular cavity depend on the assumed values for dielectric constants. Letting $\varepsilon = 80$ for the cavity as well as bulk solutions and $\varepsilon = 2$ for the membrane and protein interior in a membrane of 30 Å thickness, the effects are accounted for by a cylindrical cavity of ~25-Å depth and 3-Å radius. The calculations performed with a truncated conical cavity show that an even deeper cavity would be necessary to explain the effects of low S on gating current.

When we considered having a reduced dielectric constant ε in the internal cavity, as suggested by previous theoretical work, the geometry that incorporates an internal and an external cavity seems to provide a good explanation for both the intracellular and extracellular effects of lowered S. Meanwhile, the question remains as to what is the correct value of ε to use to describe the interior of a membrane protein. It was originally suggested that a value of 8 and as a high as 20 was necessary to account for the pK_a of soluble proteins. More recently, work that explicitly treats protein conformational changes suggested that an ε value of 4 (Havranek and Harbury, 1999) or 2 (Misra et al., 1998) is more appropriate to capture the electronic polarizability effects that contribute more significantly to the dielectric properties of a protein. Also, a recent study (Dwyer et al., 2000) shows that the large values of ε encountered in the interior of proteins, may arise from water penetration into the core of the molecule.

Validity of the Continuum Theory

The Poisson-Boltzmann equation embodies a mean-field theory, in which ion concentrations are represented by a smeared out continuum of charge. Two problems can be imagined to arise because of the mean-field approximation in the present context. First, the dimensions of the internal cavity (e.g., the one in Fig. 12) are so small that at a concentration of 24 mM, the cavity is occupied by an ion with a probability of only 0.037. At $S = 318$ mM, the occupancy increases to 0.5. It is clear that the charge measured in the external circuit will be a quantity that fluctuates as ions diffuse into and out of the cavity on a nanosecond time scale. However, this is no problem because the gating charge as a function of potential is an equilibrium quantity (at least on the time scale of a few milliseconds in our measurements) and, therefore, the time-averaged charge movement measurement is appropriate.

The other problem with the use of a mean-field theory concerns the reaction field experienced by individual ions. Although the Poisson-Boltzmann theory is quite successful in describing ion behavior in bulk solutions and also at planar interfaces (Bockris and Reddy, 1973), the theory does not describe reaction field effects as individual ions approach dielectric boundaries. Moy et al. (2000) have demonstrated a depletion of ions due to the repulsive reaction field that increases as charge squared and, therefore, is incorrectly described by a continuum of charge. We have included this effect as a depletion area around the dielectric boundary, and show that the effect may be more pronounced in the low dielectric constant internal cavity. This depletion region is similar to the volume exclusion region of 2–4 Å which is commonly used in electrostatic and molecular dynamics simulations (Alexov and Gunner, 1997; Misra et al., 1998).

Finally, it should be emphasized that we have used only the linearized form of the Poisson-Boltzmann equation. Because it is linear, this equation allows very great simplifications through superposition. We are interested only in the changes in potential due to the applied membrane potential, so that superposition allows us to neglect any effects of fixed charges in the system. It also allows us to present the computed potentials simply as fractions of the membrane potential. The linearized equation is an approximation, valid for potentials differing less than about kT/e_0 from the bulk solution potential. Very close to fixed charges, this approximation will not hold, but the polarity of the error is not obvious: at moderate electric field strengths, the screening effect is expected to be larger; but, at high field strengths, the finite ion radii and saturation of water dipoles will reduce the screening effect. Because the detailed structure of the protein is not known, we take the linearized equation as an accessible and reasonable approximation to the actual problem.

Shape of the Cavities

The exact geometry of the cavity would be expected to be much more complex than the models presented here, but the simple existence of a cavity seems to be enough to sharply focus the electric field into a small region of the protein, which is not possible in a simple

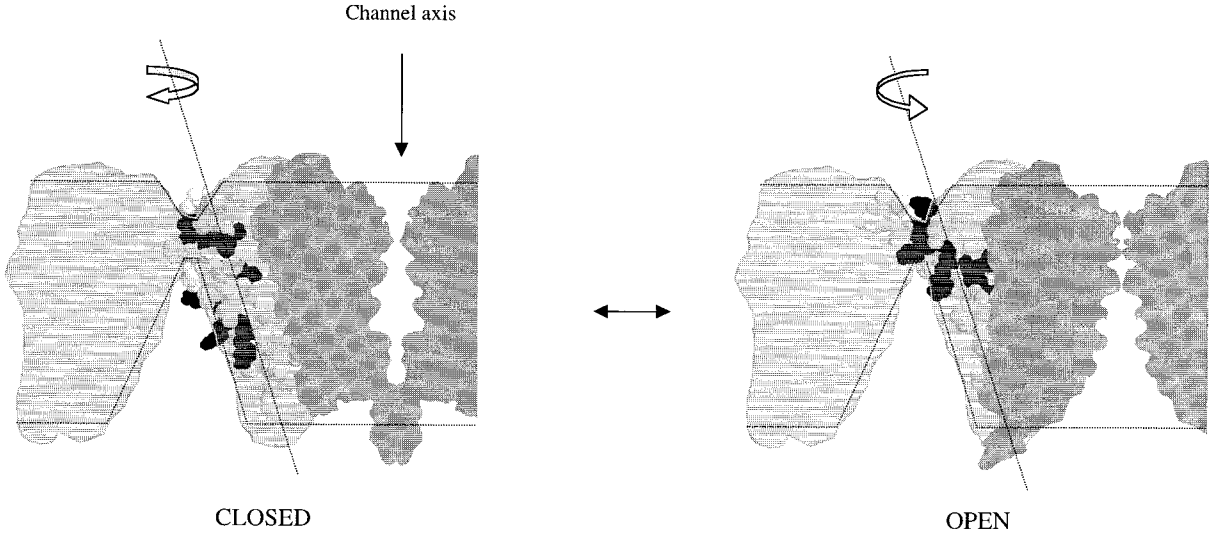

FIGURE 13. Cartoon of the possible geometry of the gating pore and voltage sensor. The S4 helix is represented by the structure proposed in the model of Durell et al. (1998) as a space-filling α-helix, the charged residues are in black. The lightly shaded area represents the bulk of the channel's voltage-sensing domain, and the darker area is the pore domain (modeled after the KcsA crystal structure). The dotted lines represent an outline of the cavity around S4 that have been idealized in the electrostatic calculation. (Left) Closed conformation; (right) open conformation. It is assumed that the main conformational change is a rotation of the S4 α-helix around its axis. Upon depolarization, a small portion of the voltage sensor moves, changing the accessibility of the NH_2-terminal charged residues that are more external. This movement of charged residues across the narrow area of focused membrane potential produces the gating currents.

planar membrane. We suggest that the internal cavity is very deep and relatively narrow while the external cavity, if any, is small. Our favorite model is an internal conical cavity of ~20-Å depth and external mouth radius of 10 Å and internal radius of 3 Å. This internal cavity is large enough to give access to the relatively large (6-Å diam by 10 Å in length) cysteine modifying agents used in other experiments (Karlin and Akabas, 1998). The cavity may be larger if the magnitude of ion repulsion effects in the dielectric boundary are considerable (up to r_m =14 Å, r_a = 6 Å, and a depth of 24 Å; Fig. 11 D). The volume of this cavity would be large enough to contain a large number of water molecules. The region of membrane potential focusing, as suggested by these calculations, may be as small as 3 Å in thickness and not larger than 10 Å. It is possible that this region is formed at the intersection of a number of the α-helices, which may form the core of one of the channel's subunits. In our favored geometry (Fig. 12), the low dielectric septum is only 3 Å thick, which is in agreement with suggestions from other experiments (Starace et al., 1997).

Fig. 13 presents a cartoon representation of one subunit of the *Shaker* channel in two conformations. The cavity would be formed by a bundle of α-helices, and one of those helices would be S4 itself. Most α-helices in bundles cross at an angle of between 11° and 20° (Chothia et al., 1981; Son and Sanson, 1999), although the helices in the KcsA channel come together at a larger angle (Doyle et al., 1999). Given the results of our electrostatic calculations with the conical cavity of reduced ε, the dimensions of the best cavity are 20 Å in the mouth opening and 6 Å at the apex. This corresponds to a crossing angle of ~40°.

Since the extracellular effects of reduced *S* are small, and the electrostatic calculations suggest that using a small (3–5 Å) external cavity is appropriate, we suggest that the helix bundle actually forms in the external third of the membrane, just opposite to the form the bundle crossing occurs in the KcsA channel, which happens in the intracellular region. This disposition would form a long internal cavity and a short external cavity (Fig. 13). In summary, this structural cartoon is consistent with the data presented here and that of other groups. It incorporates a conical cavity whose size is consistent with that of cysteine-modifying compounds. Gating charges are displaced across a thin septum, allowing a small movement, such as a helix rotation, to give rise to the large gating charge movement of >3 e_o per channel subunit.

We wish to thank Y.-Y. Yan for expert technical assistance. We thank B. Roux (Cornell Medical Center, NY, NY), and Y. Yang and Q.-X. Jiang (Yale University) for discussions and helpful comments during the course of this work.

This study was supported by the National Institutes of Health grant NS 21501 to F.J. Sigworth.

Submitted: 11 July 2000
Revised: 9 November 2000
Accepted: 5 December 2000

REFERENCES

Aggarwal, S.K., and R. MacKinnon. 1996. Contribution of the S4 segment to gating charge in the *Shaker* K^+ channel. *Neuron*. 16: 1169–1177.

Alexov, E.G. and M.R. Gunner. 1997 Incorporating protein conformational flexibility into the calculation of pH-dependent protein properties. *Biophys. J.* 74:2075–2093.

Antosiewicz, J., J.A. McCammon and M.K Gilson. 1996. The determinants of pK_as in proteins. *Biochemistry*. 35:7819–7833.

Armstrong, C.M. 1999. Distinguishing surface effects of calcium ion from pore-occupancy effects in Na^+ channels. *Proc. Natl. Acad. Sci USA*. 96:4158–4163.

Baker, O.S., H.P. Larsson, L.M. Mannuzzu, and E.Y. Isacoff. 1998. Three transmembrane conformations and sequence-dependent displacement of the S4 domain in *Shaker* K^+ channel gating. *Neuron*. 20:1283–1294.

Baukrowitz, T., and G. Yellen. 1996. Use-dependent blockers and exit rate of the last ion from the multi-ion pore of a K^+ channel. *Science*. 271:653–656.

Beece, D., L. Eisenstein, H. Frauenfelder, D. Good, M.C. Marden, L. Reinisch, A.H. Reynolds, L.B. Sorensen, and K.T. Yue. 1980. Solvent viscosity and protein dynamics. *Biochemistry*. 19:5147–5157.

Boccaccio, A., O. Moran, and F. Conti. 1998. Calcium dependent shifts of Na^+ channel activation correlated with the state dependence of calcium-binding to the pore. *Eur. Biophys. J.* 27:558–566.

Bockris, J.O.M., and A.K.N. Reddy. 1973. Modern Electrochemistry. Plenum Press, New York. Second edition. 235–250.

Campbell, D.T., and R. Hahin. 1984. Altered sodium and gating current kinetics in frog skeletal muscle caused by low external pH. *J. Gen. Physiol.* 84:771–788.

Cha, A., and F. Bezanilla. 1997. Characterizing voltage-dependent conformational changes in the *Shaker* K^+ channel with fluorescence. *Neuron*. 19:1127–1140.

Chandler, W.K., A.L. Hodgkin, and H. Meves. 1965. The effect of changing the internal solution on sodium inactivation and related phenomena in giant axons. *J. Physiol.* 180:821–836.

Chothia, C., M. Levitt, and D. Richardson. 1981. Helix to helix packing in proteins. *J. Mol. Biol.* 145:215–250.

Conti, F., and W. Stühmer. 1989. Quantal charge redistributions accompanying the structural transitions of sodium channels. *Eur. Biophys. J.* 17:53–59.

Crouzy, S.C., and F.J. Sigworth. 1993. Fluctuations in ion channel gating currents. Analysis of nonstationary shot noise. *Biophys. J.* 64:68–76.

Cukierman, S. 1991. Asymmetric electrostatic effects on the gating of rat brain sodium channels in planar lipid membranes. *Biophys. J.* 60:845–855.

Doyle, D.A., J.M. Cabral, R.A. Pfuetzner, A. Kuo, J.M. Gulbis, S.L. Cohen, B.T. Chait, and R. MacKinnon. 1998. The structure of the potassium channel: molecular basis of K^+ conduction and selectivity. *Science*. 280:69–77.

Durell, S.R., Y. Hao, and H.R. Guy. 1998. Structural models of the transmembrane region of voltage-gated and other K^+ channels in open, closed, and inactivated conformations. *J. Struct. Biol.* 121:263–284

Dwyer, J.J., A.G. Gittis, D.A. Karp, E.E. Lattman, D.S. Spencer, W.E. Sites, and E.B. Garcia-Moreno. 2000. High apparent dielectric constants in the interior of a protein reflect water penetration. *Biophys. J.* 79:1610–1620.

Elinder, F., Y. Liu, and P. Arhem. 1998. Divalent cation effects on the *Shaker* K channel suggest a pentapeptide sequence as determinant of functional surface charge. *J. Memb. Biol.* 165:183–189.

Frankenhaeuser, B., and A.L. Hodgkin. 1957. The action of calcium on the electrical properties of squid axons. *J. Physiol.* 137: 218–244.

Goldstein, S.A. 1996. A structural vignette common to voltage sensors and conduction pores: canaliculi. *Neuron*. 16:717–722.

Havranek, J.J., and P.B. Harbury. 1999. Tanford-Kirkwood electrostatics for protein modeling. *Proc. Natl. Acad. Sci. USA*. 96:11145–11150.

Heginbotham, L., and R. MacKinnon. 1993. Conduction properties of the cloned *Shaker* K^+ channel. *Biophys. J.* 65:2089–2096.

Heinemann, S.H., and F. Conti. 1992. Nonstationary noise analysis and application to patch clamp recordings. *Methods Enzymol.* 207: 131–148.

Hille, B., J.M. Ritchie, and G.R. Strichartz. 1975a. The effect of surface charge on the nerve membrane on the action of tetrodotoxin and saxitoxin in frog myelinated nerve. *J. Physiol.* 250:34P–35P.

Hille, B., A.M. Woodhull, and B.I. Shapiro. 1975b. Negative surface charge near sodium channels of nerve: divalent ions, monovalent ions, and pH. *Philos. Trans. R. Soc. Lond. B. Biol. Sci.* 270:301–318.

Hirschberg, B., A. Rovner, M. Lieberman, and J. Patlak. 1995. Transfer of twelve charges is needed to open skeletal muscle Na^+ channels. *J. Gen. Physiol.* 106:1053–1068.

Hoshi, T., W.N. Zagotta, and R.W. Aldrich. 1990. Biophysical and molecular mechanisms of *Shaker* potassium channel inactivation. *Science*. 250:533–538.

Hurst, R.S., M.J. Roux, L. Toro, and E. Stefani. 1997. External barium influences the gating charge movement of *Shaker* potassium channels. *Biophys. J.* 72:77–84.

Islas, L.D., and F.J. Sigworth. 1999. Voltage sensitivity and gating charge in *Shaker* and *Shab* family potassium channels. *J. Gen. Physiol.* 114:723–741.

Jordan, P.C., R.J. Bacquet, J.A. McCammon, and P. Tran. 1989. How electrolyte shielding influences the electrical potential in transmembrane ion channels. *Biophys. J.* 55:1041–1052.

Karlin, A., and M.H. Akabas. 1998. Substituted-cysteine accessibility method. *Methods Enzymol.* 293:123–145.

Klapper, I., R. Hagstrom, R. Fine, K. Sharp, and B. Honig. 1986. Focusing of electric fields in the active site of Cu-Zn superoxide dismutase: effects of ionic strength and amino-acid modification. *Proteins*. 1:47–59.

Larsson, H.P., O.S. Baker, D.S. Dhillon, and E.Y. Isacoff. 1996. Transmembrane movement of the *Shaker* K^+ channel S4. *Neuron*. 16:387–397.

Mannuzzu, L.M., M.M. Moronne, and E.Y. Isacoff. 1996. Direct physical measure of conformational rearrangement underlying potassium channel gating. *Science*. 271:213–216.

Misra, V.K., J.L. Hecht, A.-S. Yang, and B. Honig. 1998. Electrostatic contributions to the binding energy of the λcl repressor to DNA. *Biophys. J.* 75:2262–2273.

Moy, G., B. Corry, S. Kuyucak, and S.-H. Chung. 2000. Tests of continuum theories as models of ion channels. I. Poisson-Boltzmann theory versus Brownian dynamics. *Biophys. J.* 78:2349–2363.

Olcese, R., R. Latorre, L. Toro, F. Bezanilla, and E. Stefani. 1997. Correlation between charge movement and ionic current during slow inactivation in *Shaker* K^+ channels. *J. Gen. Physiol.* 110:579–589.

Perozo, E., R. MacKinnon, F. Bezanilla, and E. Stefani. 1993. Gating currents from a nonconducting mutant reveal open-closed conformations in *Shaker* K^+ channels. *Neuron*. 11:353–358.

Rashin, A., A.M. Iofin, and B. Honig. 1986. Internal cavities and buried waters in globular proteins. *Biochemistry*. 25:3619–3625

Rayner, M.D., J.G. Starkus, P.C. Ruben, and D.A. Alicata. 1992. Voltage-sensitive and solvent-sensitive processes in ion channel gating. Kinetic effects of hyperosmolar media on activation and deactivation of sodium channels. *Biophys. J.* 61:96–108.

Roux, B. 1997. Influence of the membrane potential on the free energy of an intrinsic protein. *Biophys. J.* 73:2980–2989.

Roux, B., and M. Karplus. 1991. Ion transport in a model gramicidin channel. Structure and thermodynamics. *Biophys J.* 59:961–981.

Sansom, M.S., G.R. Smith, C. Adcock, and P.C. Biggin. 1997. The dielectric properties of water within model transbilayer pores. *Biophys. J.* 73:2404–2415.

Schoppa, N.E., and F.J. Sigworth. 1998. Activation of *Shaker* potassium channels. III. An activation gating model for wild-type and V2 mutant channels. *J. Gen. Physiol.* 111:313–342.

Seoh, S.A., D. Sigg, D.M. Papazian, and F. Bezanilla. 1996. Voltage-sensing residues in the S2 and S4 segments of the *Shaker* K^+ channel. *Neuron.* 16:1159–1167.

Sheinerman, F.B., R. Norel, and B. Honig. 2000. Electrostatic aspects of protein-protein interactions. *Curr. Opin. Struct. Biol.* 10: 153–159.

Sigworth, F.J. 1980. The variance of sodium current fluctuations at the node of Ranvier. *J. Physiol.* 307:97–129.

Sigworth, F.J. 1994. Voltage gating of ion channels. *Q. Rev. Biophys.* 27:1–40.

Son, H.S., and M.S.P. Sanson. 1999. Simulation of the packing of idealized transmembrane α-helix bundles. *Eur. Biophys. J.* 28:489–498.

Starace, D.M., E. Stefani, and F. Bezanilla. 1997. Voltage-dependent proton transport by the voltage sensor of the *Shaker* K^+ channel. *Neuron.* 19:1319–1327.

Starkus, J.G., T. Schlief, M.D. Rayner, and S.H. Heinemann. 1995. Unilateral exposure of *Shaker* B potassium channels to hyperosmolar solutions. *Biophys. J.* 69:860–872.

Taglialatela, M., L. Toro, and E. Stefani. 1992 A novel voltage clamp to record small, fast currents from ion channels expressed in *Xenopus* oocytes. *Biophys. J.* 61:78–82.

Yang, N., and R. Horn. 1995. Evidence for voltage-dependent S4 movement in sodium channels. *Neuron.* 15:213–218.

Yang, N., A.L. George, Jr., and R. Horn. 1996. Molecular basis of charge movement in voltage-gated sodium channels. *Neuron.* 16: 113–122.

Yang, Y., Y. Yan, and F.J. Sigworth. 1997. How does the W434F mutation block current in *Shaker* potassium channels? *J. Gen. Physiol.* 109:779–789.

Zagotta, W.N., T. Hoshi, J. Dittman, and R.W. Aldrich. 1994. *Shaker* potassium channel gating. II: Transitions in the activation pathway. *J. Gen. Physiol.* 103:279–319.

Zimmerberg, J., F. Bezanilla, and V.A. Parsegian. 1990. Solute inaccessible aqueous volume changes during opening of the potassium channel of the squid giant axon. *Biophys. J.* 57:1049–1064.